Applied Surface Science 692 (2025) 162741



Contents lists available at ScienceDirect

Applied Surface Science

journal homepage: www.elsevier.com/locate/apsusc

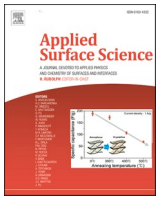

Full Length Article



Resistance of di-cationic surfactant containing pyridinium ions to metal oxidation in 1.0 M HCl medium

Serkan Öztürk [a,*], Zafer Gültekin [b], Gülşen Akgül [a], Gökhan Gece [c], Lukman O. Olasunkanmi [d,e]

[a] Department of Chemistry, Faculty of Science and Arts, Bursa Uludag University, Bursa 16059 Turkey
[b] Department of Physics, Faculty of Science and Arts, Bursa Uludag University, Bursa 16059 Turkey
[c] Department of Chemistry, Faculty of Engineering and Natural Sciences, Bursa Technical, University, 16310 Bursa, Turkey
[d] Department of Chemistry, Faculty of Science, Obafemi Awolowo University, Ile Ife 220005, Nigeria
[e] Department of Chemical Sciences, University of Johannesburg, P.O. Box 17011, Doornfontein Campus, 2028 Johannesburg, South Africa

ARTICLE INFO

Keywords:
Syntesis
Di-cationic surfactant
Corrosion inhibitor
Contact angle
DFT
Monte Carlo simulation

ABSTRACT

In order to prevent metal corrosion in low-carbon steel, which is exposed to faster corrosion in acidic environments, a di-cationic surfactant containing two pyridinium ions with high anti-corrosion potential was synthesized in this study. The structural characterization of the new compound was carried out by spectroscopic techniques (FT-IR and NMR). As a result of corrosion tests performed with electrochemical techniques such as potentiodynamic polarization (PDP) and electrochemical impedance spectroscopy (EIS) for different inhibitor concentrations (2, 10 and 50 ppm) in 1.0 M HCl solution at 25 °C, it was found that the anti-corrosion effect increases with increasing inhibitor concentration. The adsorption of the surfactant to the metal surface has been proven by the contact angles measured for pure water dripping on the metal surface. From the equilibrium constant and Gibbs free adsorption energy calculated by Langmuir adsorption isotherm, it was determined that this di-cationic surfactant has a high adsorption ability and adheres to the surface by chemical adsorption. The chemical indices of conceptual density functional theory (DFT) were also examined to develop an understanding of how molecular/electronic factors can alter inhibition efficiency of inhibitor compound. In addition to this process, a Monte Carlo Simulation study was also performed. The corrosion protection of the metal was visually examined by scanning electron microscopy (SEM) analysis, the elemental percentage of the metal surface was revealed by electron dispersive X-ray spectroscopy (EDX) analysis and the average roughness of the surface was determined by atomic force microscopy (AFM) analysis.

1. Introduction

Metals corrode as a result of chemical or electrochemical reactions that occur with their interaction with their environment [1]. In the chemical industry, environmental issues such as corrosion are one of the most fundamental areas of academic research. In particular, the type of corrosion caused by the effects of acid solution on metallic materials leads to serious material and cost losses in industry [2]. The use of corrosion inhibitors, which are necessary to solve this problem, is known as an effective, practical way to protect metal surfaces. Depending on their physical and chemical properties, the attachment of an organic inhibitor to the metal surface by adsorption is a well-known process for the protection of metal surfaces [3]. Heteroatom-containing structures such as sulfur, nitrogen and oxygen, respectively, increase the protection efficiency of organic inhibitors. Studies have concluded that the presence of multiple adsorption active centers of the inhibitor group containing unshared electron pairs and/or π orbitals, electronic density at the donor atom and its properties such as molecular size, physicochemical and planarity affect its adsorption on mild steel [4].

All metals have a tendency to transform into the mineral state in which they are found in nature, i.e. their lowest-energy form, which is their most stable state. These minerals are energized through some processes and transformed into elemental metal forms, but they are not stable enough in this form. This free energy exchange between the two states greatly affects the susceptibility of metals to corrosion.

Corrosion inhibitors are substances that significantly reduce the rate of corrosion when added to the environment to which metals are exposed. These inhibitors are used in a variety of applications such as

* Corresponding author.
E-mail address: serkanozturk@uludag.edu.tr (S. Öztürk).

https://doi.org/10.1016/j.apsusc.2025.162741
Received 18 October 2024; Received in revised form 28 January 2025; Accepted 18 February 2025
Available online 20 February 2025
0169-4332/© 2025 Elsevier B.V. All rights are reserved, including those for text and data mining, AI training, and similar technologies.

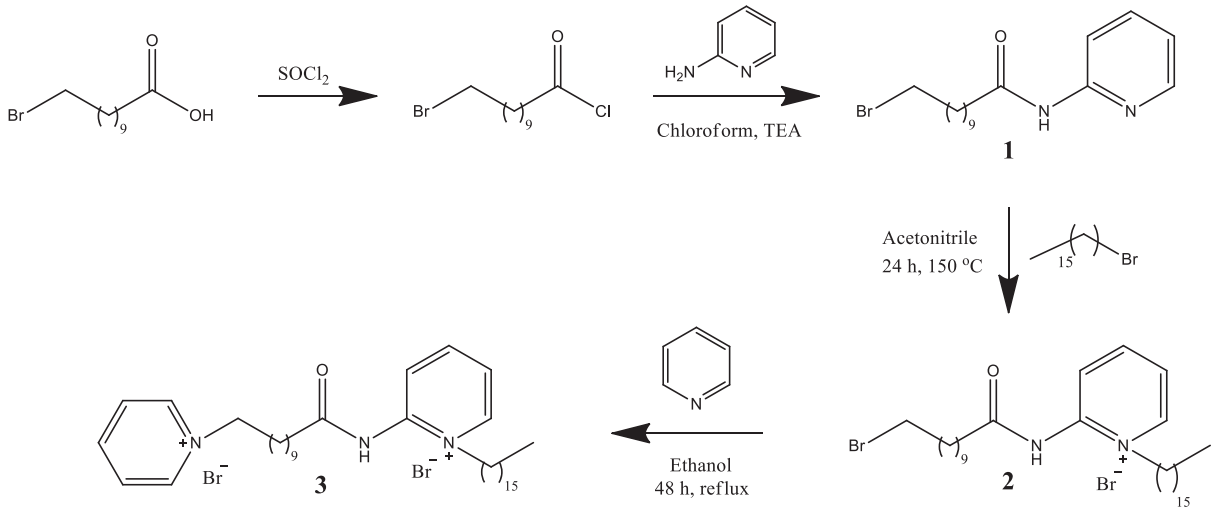

Scheme 1. Reaction steps of **HPUP (3).**

closed or open water circuits, acid solution baths and cooling systems with high water circulation rates. Inhibitors act by adsorption of ions and molecules on the metal surface, changing the rate of electrochemical reactions, reducing the rate of diffusion of corrosion-promoting reactants and increasing the electrical resistance of the metal surface. Industries where corrosion inhibitors are widely used include oil and gas exploration production, oil refining, chemical production, heavy industry, automotive industry and power plants [5].

Pyridinium salts are a very important raw material in the chemical industry. Apart from this, it has many applications in many fields such as anti-microbial, drug delivery systems, gene therapy, cosmetics, phase transfer catalyst, dyes, sensors, electrolytes, etc. [6] In some recent studies, it has been discovered that this class of compounds can inhibit metal corrosion as surfactants. It is possible to find a few studies in which compounds containing pyridinium ions were used as corrosion inhibitors in acidic media. In one of these studies, seven cationic surfactants of imidazolium, pyridinium and dimethyl-ethylbenzyl ammonium derivatives were synthesized and their inhibition activity in hydrochloric acid at different inhibitor concentrations (10, 25, 50, 100 ppm) was investigated. The corrosion inhibition was attributed to the cationic surfactants binding to the molecular structure (heterocyclic ring, hydrophobic chain length) and enhancing their adsorption on the surface of steel. In addition, Electrochemical Impedance Spectroscopy spectra were fitted using the Voigt model [7]. In a study by Shalabi et al. 2019 [8], 1-dodecyl-3-(hydroxymethyl) pyridin-1-ium bromide (DHPB) was found to be an effective corrosion inhibitor for carbon steel in 2 M HCl and its activity increased with concentration and temperature. Quantum calculations and molecular dynamics simulations showed the influence of the structure of DHPB on its activity, while SEM and AFM confirmed the carbon steel surface protection by DHPB adsorption [8]. In a different study, two surfactants containing pyridinium ions were synthesized which had inhibitory effects against carbon steel corrosion in 1.0 M HCl. It was determined that the longer chain compound exhibited higher activity. In addition, DFT calculations and SEM images supported the corrosion inhibition findings [9]. In another study, Tu et al. 2012 [4] synthesized N-alkyl-4-(4-hydroxybut-2-inyl) pyridinium bromides and evaluated their corrosion inhibition activity on X70 steel in 5 M HCl by weight loss and electrochemical methods. It has been reported that the synthesized molecules adsorb to the X70 surface by displacing water and raise the energy barrier for corrosion by blocking the active sites [4].

Computational chemistry methods are becoming omnipresent in corrosion inhibitor efficiency prediction [10]. Geometry optimization of the inhibitors within the chosen route can be performed using a myriad of approaches, including DFT. Further detailed molecular modelling studies provide additional understanding toward a robust correlation between a calculated parameter and corrosion efficiency. By unifying the experimental and computational treatments, accurate estimation of the inhibition behaviour of the potential compounds could be anticipated [11]. There are interesting studies in the literature where the correlation between the parameters obtained by DFT and other computational chemistry methods and the anti-corrosion properties of inhibitors are determined [12–15].

In this research work, it is planned to obtain a di-cationic surfactant (HPUP) containing two pyridinium rings and a long chain of 16 carbons linked to a positive nitrogen atom in one of the pyridinium rings. The corrosion rates and inhibition efficiency of this material at different inhibitor concentrations have been determined in acidic media (1.0 M HCl) where corrosion occurs very rapidly. Corrosion inhibition efficiency values have been ascertained by electrochemical measurements such as potentiodynamic polarization curves and electrochemical impedance spectroscopy, which are more sensitive and accurate than the weight loss method. The synthesis of a new surfactant containing pyridinium ion, which has a wide range of applications, and the determination of the corrosion inhibition activity of the synthesized compound in acidic media by electrochemical measurements that give more accurate and precise results make this study remarkable. The inhibition efficiency values obtained from the two methods have been compared with each other. In order to support the idea that the di-cationic surfactant adsorbs on the mild steel surface and shows anti-corrosion effect, it is aimed to measure the contact angle in pure water dropped on the metal surface after corrosion test and to perform adsorption isotherm study. In addition to these, density functional theory (DFT) and Monte Carlo simulation techniques have been used to correlate with the inhibition activity results; and scanning electron microscopy (SEM) and atomic force microscopy (AFM) images of the metal surface have been taken to support the anti-corrosive effect.

2. Materials and experimental procedures

2.1. Materials and Instrumentations

The reagents and solvents used in the synthesis and corrosion studies were purchased from Merck (Merck, Darmstadt, Germany) and were deployed without secondary purification. These reagents and solvents are 11-bromoundecanoic acid, thionyl chloride (SOCl2), toluene, 2-amino-pyridine, chloroform, acetonitrile, 1-hexadecyl bromide, pyridine, HCl (37 %) and triethylamine (TEA). Thin layer chromatography

(TLC) was performed using silica gel (60 F254, Merck, Darmstadt, Germany) plates. Perkin Elmer Spectrum Two FT-IR spectrophotometer (Shelton, Connecticut, USA) and Agilent 600 MHz Premium Compact NMR spectrometer (Santa Clara, CA, USA) in DMSO (Dimethylsulfoxide) solvent were used to obtain the FT-IR and NMR spectra (^{1}H NMR and ^{13}C NMR) of the synthesized di-cationic surfactant. A NUVE EV 018 vacuum oven (Ankara, Turkey) was used to dry the metal plates to constant weight, excluding atmospheric air. A LECO CHNS-932 elemental analyzer (Saint Joseph, MI, USA) was used for elemental content determination.

2.2. Description of synthesis

Scheme 1 shows the reaction steps.

2.2.1. Synthesis of 11-bromo-undecanoyl chloride

In a flask, 56.5 mmol of 11-bromoundecanoic acid was mixed with 28 mL of thionyl chloride in toluene solvent. The reaction mixture was stirred at room temperature for approximately 12 h. It was then heated at about 80 °C for 5 h under a reflux cooler. During this process, a $CaCl_2$ tube was attached to the head of the recooler to prevent the reaction from being affected by the environment. Then toluene and unreacted thionyl chloride were removed by evaporator.

2.2.2. Synthesis of 11-bromo-N-(pyridin-2-yl)undecanamide (1)

In a double-necked flask, 59.3 mmol of 2-aminopyridine, 74.13 mmol of triethylamine and chloroform as solvent were placed and stirred at a temperature close to boiling point. The double-necked flask was then allowed to cool. The solution of acid chloride compound in chloroform was slowly dripped into the cooled mixture through a dropping funnel. After dripping, the dropping funnel was removed and the flask was stirred for about half an hour. At the end of the time, the ice bath was removed and the double-necked flask was stirred overnight at room temperature. Then heating was carried out at 60–70 °C for about 4 h. At the end of the time, the reaction mixture was extracted with water. The organic phase was dried with Na_2SO_4. Then, the chloroform was evaporated in an evaporator. The obtained product was used for the next steps.

2.2.3. Synthesis of 2-(11-bromoundecanamido)-1-hexadecylpyridin-1-ium bromide (2)

Into a 100 mL flask were added 15.76 mmol of the amide compound 11-bromo-N-(pyridin-2-yl)undecanamide, 31.52 mmol of 16 carbon alkyl bromide (1-Bromo-hexadecane), and acetonitrile as solvent. It was refluxed at 150 °C under a reflux cooler for about 24 h. The end of the reaction was determined by thin layer chromatography. The solvent was then removed from the medium. The reaction flask was cooled to room temperature. The crude product in the reaction flask was washed 2 times with diethylether. During washing with ether, the unreacted alkyl bromide compound was removed. Finally, compound 2 was synthesized in 30.4 % yield.

2.2.4. Synthesis of 1-hexadecyl-2-(11-(pyridin-1-ium-1-yl)undecanamido) pyridin-1-ium di-bromide (HPUP) ($C_{37}H_{63}Br_2N_3O$) (3)

Compound **2**, pyridine and ethanol as solvent were added to the reaction flask with the same molar ratio (4.26 mmol). The reaction mixture was heated under reflux for 48 h. The progress of the reaction was monitored by TLC. The ethanol was removed in an evaporator after the time was over and the remaining substance was rinsed in a mixture of acetone-diethyl ether (about 1–4). A brown, oily wax-like product that dissolved well in water was the result of the washing process. The yield was 2.07 g (67 %).

2.3. Evaluation of material degradation in a hydrochloric acid solution with a concentration of one molar

2.3.1. Metal plates used and their preparation

The corrosion tests in acidic media involved metal plates that had low carbon content and were cold rolled steel. The steel material, which consists of 0.07 % C, 0.35 % Mn, 0.015 % P, 0.015 % S and the rest Fe, was prepared according to DIN EN 10130 [16] for the corrosion tests in acidic media. The XRD pattern of this steel material was given in Fig. S.1 (see Appendix A. Supporting information). Rectangular metal plates with dimensions of 0.1 cm thickness, 2.2 cm width and 5.0 cm length were used for the corrosion tests in acidic media. The method reported by Öztürk 2018 [17] was followed in the preparation of metals for corrosion tests. To eliminate any rust and oxide layers, the metal plates with dimensions of 0.1 × 2.2 × 5.0 cm (thickness × width × length) were immersed in a solution of 15 % HCl for 5 min. Distilled water was used to clean the metal coupons. The metal plates were dried and then their surface was smoothed with sandpaper (320–800–1500). They were then placed in acetone for a while. The metal plates were taken out of the acetone and then dried in a vacuum oven (NUVE EV 018 vacuum oven, Ankara, Turkey)..

The corrosion tests used a 1.0 M HCl solution that was freshly made before the tests. The surfactant with a double positive charge were dissolved in 100 mL of 1.0 M HCl after weighing them. They were then transferred to glass containers with lids that had a capacity of 150 mL. The inhibitors were prepared in acidic medium with concentrations of 2, 10 and 50 ppm. Another glass container had 100 mL of 1.0 M HCl for the control test and comparison, and it did not have any inhibitor.

2.3.2. Electrochemical measurements

In this research, we conducted electrochemical corrosion tests, including Open Circuit Potential (OCP), Tafel Extrapolation and Electrochemical impedance spectroscopy (EIS), on our samples using the VersaSTAT 4 galvanostat/potentiostat device (TN, USA). The device utilizes VersaStudio software for PDP experiments [9]. Electrochemical measurements were carried out using a standard three-electrode electrochemical cell, with the working electrode being a prepared metal plate that meets DIN EN 10130 standards and has an exposed area of 1.0 cm2. Prior to the corrosion test, the metal plate's surface intended for exposure to the corrosive solution was sanded with various grades of emery paper, degreased using acetone, rinsed with ultrapure water, and subsequently dried. The metal plate, serving as the working electrode, was wrapped in polyimide Kapton tape, leaving only a 1.0 cm2 area exposed to the solution. A saturated calomel electrode (SCE) was used as the reference electrode, while a platinum plate served as the counter electrode. The experiments were conducted at a stable temperature of 25 ± 1 °C [18]. During the measurements, the system was monitored for a sufficient period (1 h) to allow stabilization. Potentiodynamic polarization measurements were performed after 3600 s of open circuit potential (OCP) measurements at 0.5 s per point. Each test was performed twice under identical conditions, and the data were analyzed using VersaStudio software. During the PDP experiments, the steel surface was scanned at a rate of 5 mV/s, maintaining a constancy criterion of 4.5 μV/s, within a range of −200 to + 200 mV (vs OCP) relative to the corrosion potential (E_{corr}). This was done in both of the solution without inhibitor and solutions containing 2, 10, and 50 ppm of the inhibitor. The polarization parameters related to the corrosion process were derived by extrapolating the linear segments of the anodic and cathodic branches of the polarization curves.

Electrochemical impedance spectroscopy (EIS) data were used to determine the effects of inhibitor concentrations on corrosion. EIS measurements were taken over a wide frequency range (100 kHz −0.01 Hz) and presented as Nyquist diagrams. The evaluation of the obtained EIS data and the determination of circuit elements (double-layer capacitance (C_{dl}), charge transfer resistance (R_{ct}), and solution resistance (R_s) were performed using ZsimpWin software.

2.4. Contact angle measurements

Static pure water contact angle measurements were performed at room temperature with a commercially available contact angle measurement system. A KSV Attention Theta instrument (Hamburg, Germany) was employed to measure the contact angles of the surfaces of the metal stripes. Before contact angle measurements were performed, the metal coupons were stored in a vacuum desiccator to prevent possible corrosion due to moisture in the air. The metal coupons had been tested for inhibition in acidic medium at room temperature for 6 and 24 h. One of the metal plates was immersed in 100 mL HCl solution of molarity one without inhibitor for 6 h, while the other plate was immersed for 24 h. The metal plates were likewise immersed in HCl solutions containing 50 ppm inhibitor HPUP (**3**) separately for 6 and 24 h, respectively. After that, the metal plates were taken out of the acid solutions and dried in a vacuum desiccator until no moisture remained. By using the sessile drop method, the contact angles of the surfaces were determined. A syringe was used to drop 1 water drop onto the surface of the metal stripe. The angle of contact was measured at both ends of the drop of water that was placed on a completely dry metal surface. Each drop of water had a volume of 10 μL and was contained by the syringe. The contact angle values were measured for each drop from 15 different photos taken from various parts of the surfaces. The left and right contact angles were measured from the contact points of the droplet with the solid on the left and right sides, respectively. The average of two values was used to obtain the average contact angle values. The mean and standard deviation of these measurements were then computed [19].

2.5. SEM and EDX analysis

SEM was performed to obtain more information about the corrosion process. The metal sheets were cleaned and dried after removal from acid solutions with or without inhibitors and immediately after the corrosion test according to the weight loss method, 1000-fold magnified surface images of the metals were taken by Scanning Electron Microscopy (SEM) [Carl Zeiss / Gemini 300]. The chemical composition of the surfaces was analysed by electron dispersive X-ray spectroscopy (EDX).

2.6. AFM study

Specimens were prepared similarly to SEM samples to determine the surface roughness using AFM. However, they were gently washed with running water and acetone, then dried in warm air after being retrieved from test solutions before analysis [20]. The AFM analysis was conducted using an Ambient AFM/MFM (Nanomagnetics Instruments, Oxford, UK) model atomic force microscope.

Table 1
The characterization results of the synthesized surfactant.

Compound	Characterization data
HPUP (3)	**FT-IR (ATR, $\tilde{\nu}$/cm − 1):** 3397 (amide, N–H), 3091 (aromatic C–H), 3061 (aromatic C–H), 2924 and 2853 (aliphatic C–H), 1663 (amide C=O), 1432 (amide C–N). **^{1}H NMR (600 MHz, DMSO–d6): δ (ppm)** = 10.49 (1H, amide, N–**H**), 914, 8.14, 8.00, 7.76 (4H, aromatic C–H, O=C–NH–Py–**H**), 8.96, 8.09, 7.83 (5H, aromatik C–H, –CH_2–CH_2–Py–**H**), 4.61 (2H, CH_2, O=C–NH–PyN^+–C**H**$_2$), 4.14 (2H, CH_2, PyN^+–C**H**$_2$–CH_2), 2.47 (2H, CH_2, –CH_2–C**H**$_2$–(C=O)–NH), 2.35 (2H, CH_2, –C**H**$_2$–CH_3), 1.87 (2H, CH_2, O=C–NH–PyN^+–CH_2–C**H**$_2$), 1.63 (2H, CH_2, C**H**$_2$–CH_2–C=O), 0.80 (3H, C**H**$_3$). **13C NMR (150 MHz, DMSO–d6): δ (ppm)** = 172.90 (1C, **C**=O), 147.57, 144.51, 142.52, 128.50, 119.64 (5C, O=C–NH–Py–**C**), 145.90, 145.17, 145.07, 140.43, 136.24 (5C, –CH_2–CH_2–Py–**C**), 61.09 (1C, PyN^+–**C**H$_2$–CH_2), 53.41 (1C, O=C–NH–PyN^+–**C**H$_2$), 46.03 (1C, –CH_2–**C**H$_2$–(C=O)–NH), 14.37 (1C, –CH_2–**C**H$_3$). **Anal. Calcd for $C_{37}H_{63}Br_2N_3O$ (MW = 725,72 g / mol):** C, 61.23; H, 8.75; N, 5.79. Found: C, 61.34; H, 8.86; N, 5.70.

2.7. DFT

To meliorate our percipience of the corrosion inhibition of HPUP molecule, we implemented DFT calculations employing the B3LYP functional and the 6–311++G(d,p) basis set within Gaussian 09 W software [21]. We explored the relation between corrosion inhibition effectiveness and electronic and structural properties through reactivity molecular descriptors, including the energy value of the highest occupied molecular orbital (E_{HOMO}), the energy value of the LUMO (E_{LUMO}), the HOMO-LUMO energy difference (ΔE), the ionization potential (I), the electronegativity (χ), the electron affinity (A), the global softness (σ), the global hardness (η), the global electrophilicity index (ω), nucleophilicity index (ε), electron accepting power (ω^-), electron donating power (ω^+), and the fraction of electrons transferred (ΔN). Each descriptor is calculated by the following equations defined within the scope of conceptual DFT;

$$\mu = \left(\frac{\partial E}{\partial N}\right)_{\nu(\vec{r})} \approx -\frac{(I+A)}{2} = \frac{E_{LUMO}+E_{HOMO}}{2} = \chi \quad (1)$$

$$\eta = \left(\frac{\partial^2 E}{\partial N^2}\right)_{\nu\left(\vec{r}\right)} = \left(\frac{\partial \mu}{\partial N}\right)_{x_\nu\left(\vec{r}\right)} = \frac{E_{LUMO}-E_{HOMO}}{2} \quad (2)$$

$$\sigma = (2\eta)^{-1} = \frac{1}{(I-A)} \quad (3)$$

$$\omega = \frac{\mu^2}{2\eta} = \frac{(I+A)^2}{4(I-A)} \approx \frac{(E_{LUMO}+E_{HOMO})^2}{4(E_{LUMO}-E_{HOMO})} \quad (4)$$

$$\varepsilon = \frac{1}{\omega} \quad (5)$$

$$\omega - = \frac{(3I+A)^2}{16(I-A)} \quad (6)$$

$$\omega + = \frac{(I+3A)^2}{16(I-A)} \quad (7)$$

$$\Delta N = \frac{\phi_{Fe} - \chi_{inhibitor}}{2(\eta_{Fe}+\eta_{inhibitor})} \quad (8)$$

where μ is the Lagrange multiplier associated with the normalization constraint of DFT identified as the electronic chemical potential, E is the total energy, and ν is the external potential. In agreement with Koopmans' theorem, I and A are the vertical ionization potential and electron affinity of the system respectively, and given as I = -E_{HOMO} and A = $-E_{LUMO}$, keeping the external potential fixed. In Eq. (8), the work function Φ presents the theoretical value of electronegativity of iron ($\Phi = \chi_{Fe}$ = 4.82 eV), and the global hardness corresponds to the metallic bulk (η_{Fe} = 0 eV) [22].

2.8. Monte-Carlo simulation

The behaviour of compound **3** as inhibitors of low carbon steel in 1.0 M HCl could further be described using Monte Carlo simulation (MCS). Low carbon steel, being essentially iron (Fe) was represented by Fe (110) cleaved surface, which is the most energetically favoured crystal surface of Fe [23–25]. Ground state optimization of molecular geometry of 3 was achieved using the Forcite module contained in the Materials Studio version 7.0. The Forcite geometry optimization settings invoked in the calculations include the use of Universal forcefield, Smart algorithm, and cut-off values of 1.0 × 10^{-4} kcal/mol, 0.005 kcal/mol/Å, and 5.0 × 10^{-5} Å for energy, force and displacement, respectively. The Fe (110) plane was expanded to a 6-layered 10 × 10 supercell, over which a vacuum slab of 20 Å thickness was built. Optimized structure of the inhibitor was made to adsorb on the Fe (110) by invoking the simulated

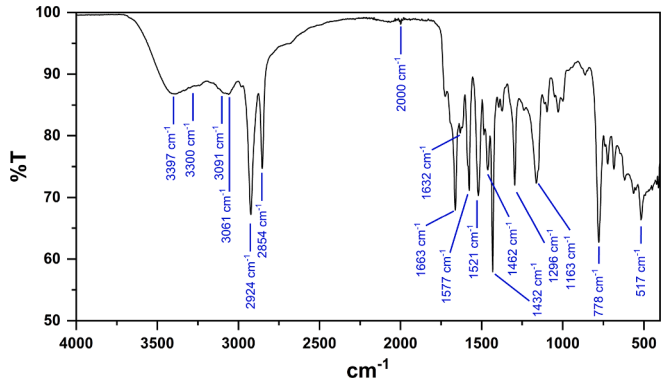

Fig. 1. FT-IR spectrum of **HPUP (3).**

annealing adsorption locator module in the Materials Studio 7.0. Adsorption of HPUP on Fe (110) was performed in the absence and presence of 20 molecules or units of H_3O^+ and Cl^- ions as corrosion ions. The medium quality settings of the simulated annealing was employed, which implies that the annealing went through 3 cycles at 15,000 steps per cycle under automated temperature control of 100,000.0 K maximum temperature and 100.0 K minimum temperature.

3. Results and discasion

3.1. Synthesis and spectroscopic analysis of compound 3

The novel di-cationic surfactant (HPUP), which is studied as a corrosion inhibitor, was synthesized in four-stage reaction steps (see Scheme 1). The characterization results of the synthesized surfactant are given in Table 1, respectively. It is possible to explain the characteristic peak values seen in the spectra as follows. In the FT–IR spectrum given in Fig. 1, the peak at 3397 cm^{-1} is the amide N–H bond stretching, the peak at 3091 cm^{-1} is the aromatic C–H stretching belonging to the pyridinium at the left end, and the peak at 3061 cm^{-1} is the aromatic C–H stretching belonging to the amide bonded pyridinium group. The peaks at 2924 cm^{-1} and 2853 cm^{-1} belong to the aliphatic C–H stretching, the peak at 1663 cm^{-1} belongs to the C=O stretching in carbonyl on the amide bond and finally the peak at 1432 cm^{-1} belongs to the C–N stretching on the amide bond. As seen in the proton NMR spectrum (Fig. 2), the peak at approximately 10.49 ppm belongs to the hydrogen in the N–H bond of the amide functional group; peaks at 9.14, 8.14, 8.00 and 7.76 ppm belong to the hydrogens of the C–H bond in the pyridinium ring to which the amide functional group is attached; peaks at 8.96, 8.09 and 7.83 ppm belong to the hydrogens of the C–H bond in the pyridinium ring at the end. Apart from these, peaks belonging to the hydrogens of the CH_2 group attached to the positively charged nitrogen atom in the pyridinium ring attached to the amide functional group at 4.61 ppm; hydrogens of the CH_2 group attached to the pyridinium nitrogen at 4.14 ppm; and hydrogens of the CH_2 group adjacent to the amide carbonyl (C=O) group at 2.47 ppm are observed. Finally, peaks belonging to the underlined hydrogens of CH_3–$\underline{CH_2}$, O=C–NH–PyN^+–CH_2–$\underline{CH_2}$, $\underline{CH_2}$–CH_2–C=O and $\underline{CH_3}$ groups appeared at 2.35, 1.87, 1.63 and 0.80 ppm, respectively. In the C-NMR spectrum of the same substance given in Fig. 3, the peak belonging to the carbonyl carbon is at 172.90 ppm; the peaks belonging to the carbon atoms in the pyridinium ring at the end are at 145.90, 145.17, 145.07, 140.43 and 136.24 ppm; the peaks belonging to the carbon atoms in the pyridinium ring connected to the amide functional group are at 147.57, 144.51, 142.52, 128.50 and 119.64 ppm. Besides these, other characteristic carbon atoms, such as the peak of CH_2 carbon bonded to the pyridinium nitrogen at the end at 61.09 ppm; the peak of CH_2 carbon bonded to the pyridinium nitrogen attached to the amide functional group at 53.41 ppm; the peak of CH_2 carbon adjacent to the carbonyl group at 46.03 ppm and the peak of CH_3 carbon at the very end of the long chain at 14.37 ppm.

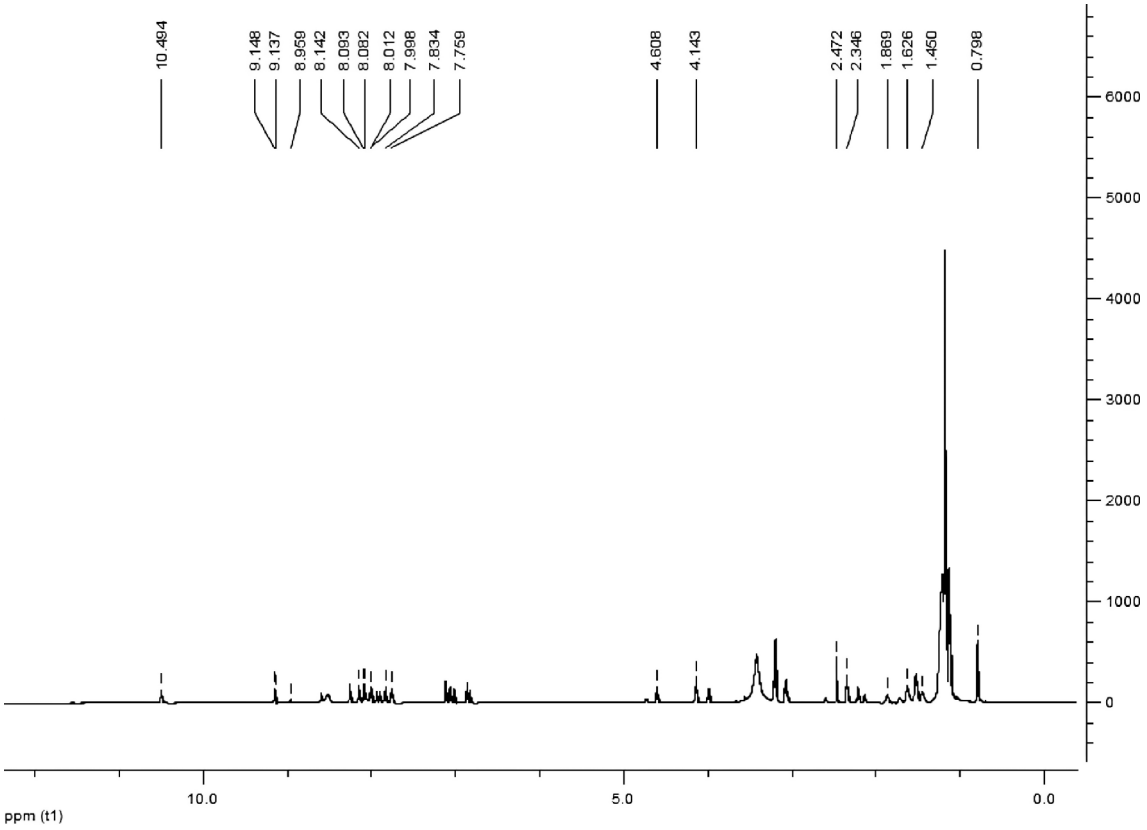

Fig. 2. ^{1}H NMR spectrum of **HPUP (3).**

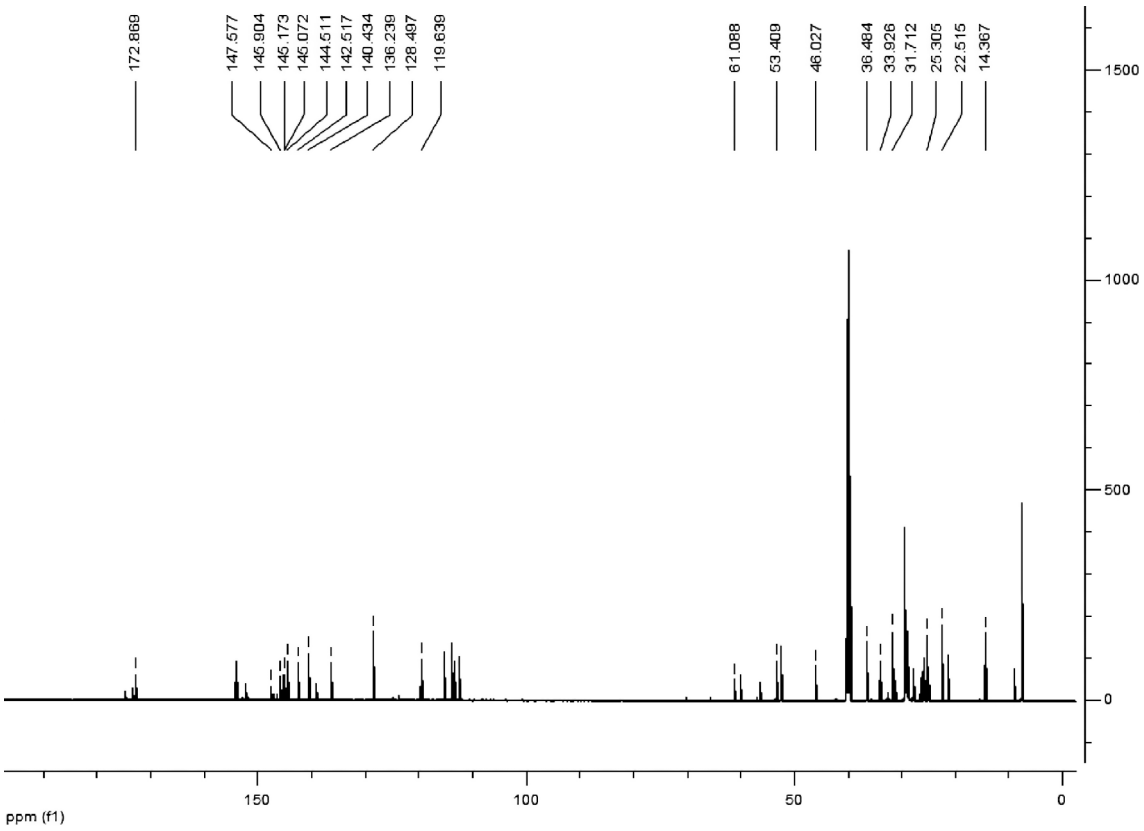

Fig. 3. ^{13}C NMR spectrum of **HPUP (3).**

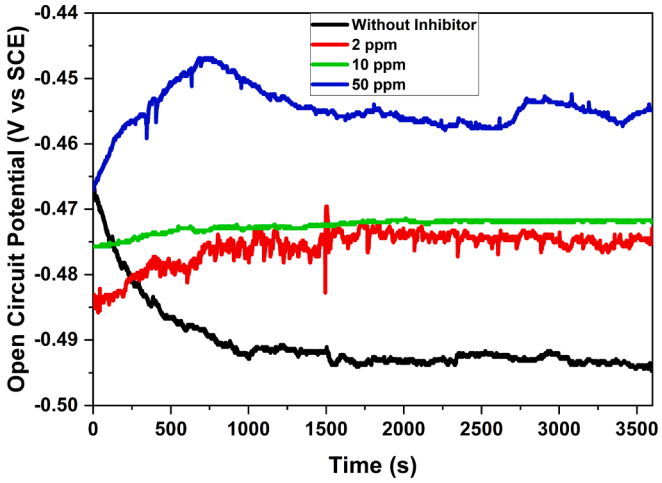

Fig. 4. E_{OCP} versus time curves for mild steel in 1.0 M HCl solution at 25 °C in absence and presence of different concentrations of HPUP.

3.2. Corrosion inhibition performance by the surfactant 3

3.2.1. Open circuit potention

OCP measurements were performed to determine the passivation properties acquired by the metal surface in a corrosive environment through the use of inhibitors. The measurements revealed how the potential changed over time, depending on the inhibitor concentrations, and demonstrated the effectiveness of inhibitors in slowing down the corrosion rate.

OCP graph given in Fig. 4 shows the potential changes of metal surfaces without inhibitor and at different inhibitor concentrations (2 ppm, 10 ppm, 50 ppm) over time. The black curve on the graph represents the open circuit potential of the metal when no inhibitor is used. The potential, which initially hovers around −0.465 V, quickly drops to more negative values in a short time, falling to −0.491 V in approximately 1500 s. This decrease indicates that corrosion reactions on the metal surface are rapidly starting and progressing. The shift in the potential towards the negative indicates that the metal is more prone to anodic dissolution and is vulnerable to corrosion. The red curve is obtained with an inhibitor concentration of 2 ppm. In this case, the OCP remains constant around −0.475 V from the beginning. This indicates that the low inhibitor concentration slows down the corrosion on the metal surface, but does not form a sufficient inhibitor layer to provide effective protection. The fact that the OCP remains almost constant indicates that the corrosion rate in the system is very low but not completely stopped. The green curve shows the OCP values obtained when 10 ppm inhibitor concentration is used. At this concentration, OCP remains constant around −0.472 V, indicating that corrosion responses are slower. It is understood that the potential is quite stable in the presence of 10 ppm inhibitor and provides more effective protection on the metal surface. At the highest inhibitor concentration of 50 ppm, the OCP is initially around −0.465 V and shifts towards more positive values over time and stabilizes around −0.454 V. The shift of the OCP to more positive values indicates that the metal becomes more resistant to corrosion and a strong inhibitor layer is formed on the surface. This result clearly reveals that the inhibitor molecules rapidly adsorb onto the surface, inhibit anodic dissolution, and greatly reduce the corrosion rate.

3.2.2. Electrochemical impedance spectroscopy

After determining the OCP measurements, electrochemical impedance measurements were made since during electrochemical impedance measurements the adjusted 1.0 cm^2 surface area has not been damaged. However, in the Tafel extrapolation method, the metal surface suffers damage due to corrosion.

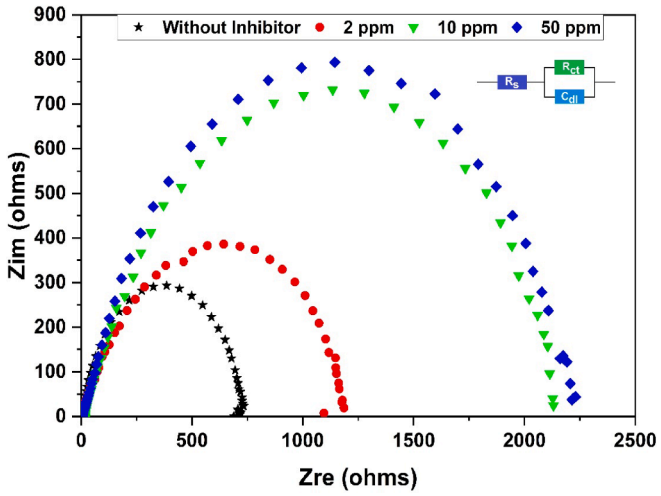

Fig. 5. Electrochemical impedance spectrum according to Nyquist format for mild steel at 25 °C in 1.0 M HCl solution without HPUP and with various concentrations of HPUP.

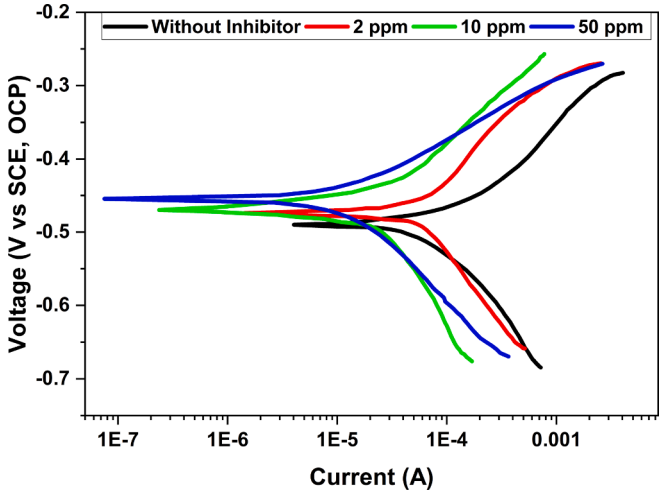

Fig. 6. Potentiodynamic polarization curves obtained for mild steel in 1.0 M HCl solution devoid and containing various concentrations of HPUP at 25 °C.

Table 2
EIS parameters for mild steel in 1.0 M HCl solution in the absence and presence of the different concentration of HPUP at 25 °C.

Concentration	R_s (Ω)	C_{dl} (μF)	R_{ct} (Ω)	X^2 (x 10^{-3})	η_{EIS} (%)
Blank	4.29	11.2	680	5.87	–
2 ppm	8.73	8.47	1032	3.73	34.1
10 ppm	12	5.6	2230	4.94	69.5
50 ppm	22	1.1	19,186	9.30	96.5

Fig. 5 shows the effect of different inhibitor concentrations (2 ppm, 10 ppm, 50 ppm) on the metal surface, along with the uninhibited case. The first scenario examined is the corrosion resistance of the metal surface without the inhibitor. In this case, the impedance exhibited by the metal is quite low, clearly indicating that the metal shows low resistance to corrosion. The short semicircular arc on the Zre axis indicates that corrosion occurs rapidly on the metal surface.

When the inhibitor is present (2 ppm), an increase in impedance values is observed. The widening of the arc shows that the inhibitor begins to form a protective layer on the metal surface, reducing the rate of corrosion. However, it is evident that at this concentration, the inhibitor is not fully effective, and higher concentrations are required for greater protection. When the inhibitor concentration is increased to 10 ppm, a significant increase in impedance values occurs. This increase indicates that the inhibitor is more densely adsorbed onto the surface, preventing corrosion reactions and significantly increasing corrosion resistance. The wider semicircular arcs indicate that the charge transfer resistance (R_{ct}) has increased substantially, and the corrosion process has slowed down. When the inhibitor concentration is raised to 50 ppm, a much larger increase in impedance values is observed. This suggests that almost a complete protective layer has formed on the metal surface, significantly inhibiting corrosion reactions. The width of the semicircle clearly demonstrates that the corrosion rate has been reduced to very low levels and that the inhibitor is highly effective.

The parameters presented in Table 2 are provided to gain a deeper understanding of how corrosion resistance on the metal surface changes depending on the presence and concentration of the inhibitor. The values of R_s, representing the resistance of the electrolyte solution, show a slight increase with inhibitor concentration. This increase is due to the effect of the inhibitor molecules on the electrical conductivity of the electrolyte solution. The double-layer capacitance (C_{dl}) represents the capacity formed by the charges accumulated on the metal surface. While the C_{dl} value is 11.2 μF in the uninhibited case, this value decreases in the presence of the inhibitor. As the inhibitor molecules adsorb onto the metal surface, the decrease in double-layer capacitance is an expected result. This shows that the inhibitors adsorb onto the surface, limiting the access of reactive ions to the metal surface and slowing down corrosion.

The charge transfer resistance, which is one of the most critical parameters determining the rate of corrosion reactions on the metal surface, is significantly increased in the presence of the inhibitor. While R_{ct} values are determined as 680 Ohms in the uninhibited case, these values increase significantly with the inhibitor. Especially at a 50 ppm inhibitor concentration, the R_{ct} value rises to 19,186 Ohms, indicating very high corrosion resistance on the metal surface. This increase clearly demonstrates that the inhibitor covers the metal surface, significantly blocking corrosion reactions. Another parameter presented in Table 2 is the inhibitor efficiency (η_{EIS}). η_{IES} indicates how effectively the inhibitor prevents corrosion on the metal surface. The η_{EIS} values of HPUP given in Table 2 were calculated using Equation (9) [26]. While the efficiency is 34.1 % at 2 ppm, this value rises to 96.5 % at 50 ppm. This result shows that as the inhibitor concentration increases, the efficiency of corrosion prevention also increases significantly.

$$\eta_{EIS}(\%) = \left(\frac{R_{ct(inhibited)} - R_{ct(Blank)}}{R_{ct(inhibited)}}\right) x100 \quad (9)$$

3.2.3. Tafel polarization curves

The Tafel plot in Fig. 6 presents the current–voltage relationship observed on the metal surface at different inhibitor concentrations (0, 2 ppm, 10 ppm, 50 ppm). The graph reveals the behavior of the curves in both the anode and cathode region, allowing the calculation of important parameters such as corrosion current density (I_{corr}) and corrosion potential (E_{corr}).

When the first case without inhibitor (black line) was examined, a high corrosion current density was observed on the metal surface. E_{corr} value was calculated as −0.491 V and I_{corr} value as 1.4×10^{-4} A/cm^2. This result indicates that the metal is highly susceptible to corrosion in the inhibitor-free environment and the corrosion rate is high. In the presence of 2 ppm inhibitor, a significant decrease in corrosion current density was observed ($I_{corr} = 8.9 \times 10^{-5}$ A/cm^2). The corrosion potential showed a slight negative shift (E_{corr} = -0.475 V). In this case, the inhibitor started to reduce the corrosion rate on the metal surface, but its effectiveness is not yet at the desired level. This is probably because it did not cover the surface completely [19]. In the presence of 10 ppm inhibitor, the corrosion current density decreased further and the Icorr value decreased to 3.8×10^{-5} A/cm^2. Ecorr value was calculated as

Table 3
Potentiodynamic polarization parameters for mild steel in 1.0 M HCl solution in the absence and presence of the different concentration of HPUP at 25 °C.

Concentration	E_{corr} (V)	I_{corr} (A/cm^2)	CR (μm/year)	η_{PDP} (%)
Blank	−0.491	1.4×10^{-4}	0.248	–
2 ppm	−0.472	8.9×10^{-5}	0.157	36.4
10 ppm	−0.475	3.8×10^{-5}	0.067	72.9

−0.472 V. In this curve, it is observed that corrosion is further controlled by the inhibitor and the metal surface is protected. At the highest inhibitor concentration of 50 ppm, the corrosion current density reached a minimum (I_{corr} = 1.0 × 10^{-5} A/cm^2). The corrosion potential was recorded as −0.454 V. In this case, it is clear that the inhibitor forms a strong protective layer on the metal surface and corrosion is almost completely inhibited.

The parameters given in Table 3 clearly show the effects of inhibitor concentrations on corrosion rate and protection efficiency. A shift in the corrosion potential to more positive values is observed as the inhibitor concentration increases. This indicates that the corrosion reactions on the metal surface are inhibited and the anode reactions are slowed down. Corrosion current density shows a significant decrease with increasing inhibitor concentration. Icorr value, which was 1.4×10^{-4} A/cm^2 without inhibitor, decreased to 1.0 × 10^{-5} A/cm^2 with 50 ppm inhibitor. This result confirms that the inhibitor effectively inhibits corrosion reactions by adsorbing on the metal surface.

As seen in Table 3, the corrosion protection efficiency increases in direct proportion to the inhibitor concentration. At 2 ppm concentration the inhibitor efficiency was 36.4 %, while at 50 ppm concentration this value increased up to 92.9 %. This indicates that the inhibitor provides more effective protection as the concentration increases, forming a denser layer on the surface. The corrosion rate was significantly reduced in the presence of inhibitor. While the corrosion rate was 0.248 μm/year without inhibitor, this value decreased to 0.018 μm/year with 50 ppm inhibitor. This result clearly shows that the inhibitor greatly reduces the corrosion rate by forming a protective layer on the metal surface. Looking at Table 3, from the corrosion test results for inhibitor 3 at different concentrations, it can be concluded that the corrosin rate decreases and the percentage inhibition efficiency increases as the concentration increases, based on the idea that the amount of material adhered to the surface will increase as the concentration increases [27–29]. These inhibition efficiency (η_{PDP}) and corrosion rate (C.R.) values given in Table 3 were calculated according to Equations (10) and (11) [30,31], respectively.

$$\eta_{PDP} = \frac{i_0 - i_{corr}}{i_0} x100 \quad (10)$$

where i_0 and i_{corr} is the corrosion current density of the samples without or with the film respectively.

$$CR = \frac{I_{corr} M}{FzD} \quad (11)$$

where M is the molecular weight, F is the Faraday's constant, z is the metal's valence and D is the density of the metal.

The presence of an inhibitor in the acid solution affects the anodic and cathodic branches. The fact that the inhibitor used affected both branches indicates a mixed type of corrosion inhibition [32]. The mixed type of inhibitory behavior can be explained as follows. In the blank acid solution, anions such as Cl^- ions are attracted to the anode (positive), while cations such as H + ions are attracted to the cathode (negative) [33]. Thus, the oxidation–reduction reactions take place complimentarily. Synthesized di-cationic surfactant has Br^- and pyridinium cationic ($N^{+)}$ moieties. Hence, in the HCl solution containing inhibitor, the Br^- competes with Cl^- for adsorption at the anode and the N^+ competes at the cathode. Br^- is more susceptible to adsorption than Cl^- because the

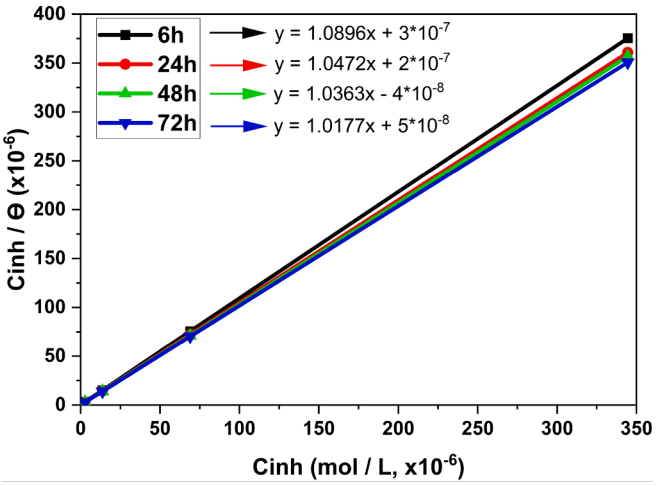

Fig. 7. Langmuir adsorption plots obtained from mass loss values for carbon steel exposed to different immersion times in 1.0 M HCl in the presence of different concentrations of di-cationic surfactant.

atomic radius of the bromine atom is greater than that of chlorine while its electronegativity is less [33], so the anode will be better populated by Br- adsorption and this will promote more HPUP adsorption through coulombic electrostatic attraction. The structure of HPUP also contains an O atom containing an electron pair and two pyridinium rings containing pi-electrons. The compound can donate these electron pairs to the d-orbital of Fe [34]. Due to the greater adsorption ability of the bromide ion and the donor–acceptor interactions in the anodic region where the corrosion event takes place, it produces a strong corrosion inhibitory effect.

3.3. Adsorption Isoterm

The corrosion inhibition mechanism can be understood by studying how molecules bind to the metal surface's active sites. Adsorption isotherm experiments reveal the nature of this molecular binding. Organic inhibitors prevent corrosion by displacing water molecules that are attached to the metal surface. This is the accepted view of how they work. There are two modes of adsorption for organic inhibitor molecules on a metal surface. The two types of adsorption are electrostatic and chemical. The former involves physical attraction, while the latter involves chemical bonding [35–37].

The Langmuir isotherm showed the best fit among the different standard adsorption isotherms. This is because the Langmuir isotherm plots had the highest linear correlation coefficient ($R^2 = 1$). These graph is shown in Fig. 7. As the Langmuir model fits the data, the adsorption of cationic surfactant on the low carbon steel surface in 1.0 M HCl solution is likely a monolayer adsorption [38].

The Langmuir adsorption isotherm is characterized by equation (12) [39].

$$\frac{C_{inh}}{\theta} = \frac{1}{K_{ads}} + C_{inh} \quad (12)$$

The weight loss values obtained are used to calculate the surface coverage (θ), which is the fraction of the surface occupied by the inhibitor molecules in M. The adsorption–desorption equilibrium constant (K_{ads}) and the inhibitor concentration (C_{inh}) are related to the surface coverage by equation (13) [40].

$$\theta = \left(\frac{W_0 - W}{W_0}\right) \quad (13)$$

W_0 is the weight loss of metal in corrosive solution without inhibitor, W is the weight loss of metal in corrosive solution with inhibitor. Fig. 7

Table 4
Adsorption equilibrium constants (K_{ads}) and Gibbs free energy values (ΔG^0_{ads}) of compounds **3** determined according to Langmuir isotherm.

Surfactants	K_{ads} (x 10^5 M^{-1})				ΔG^0_{ads} (kj mol^{-1})			
3	6 h	24 h	48 h	72 h	6 h	24 h	48 h	72 h
	36.32	52.36	259.01	203.54	−47.38	−48.28	−52.25	−51.65

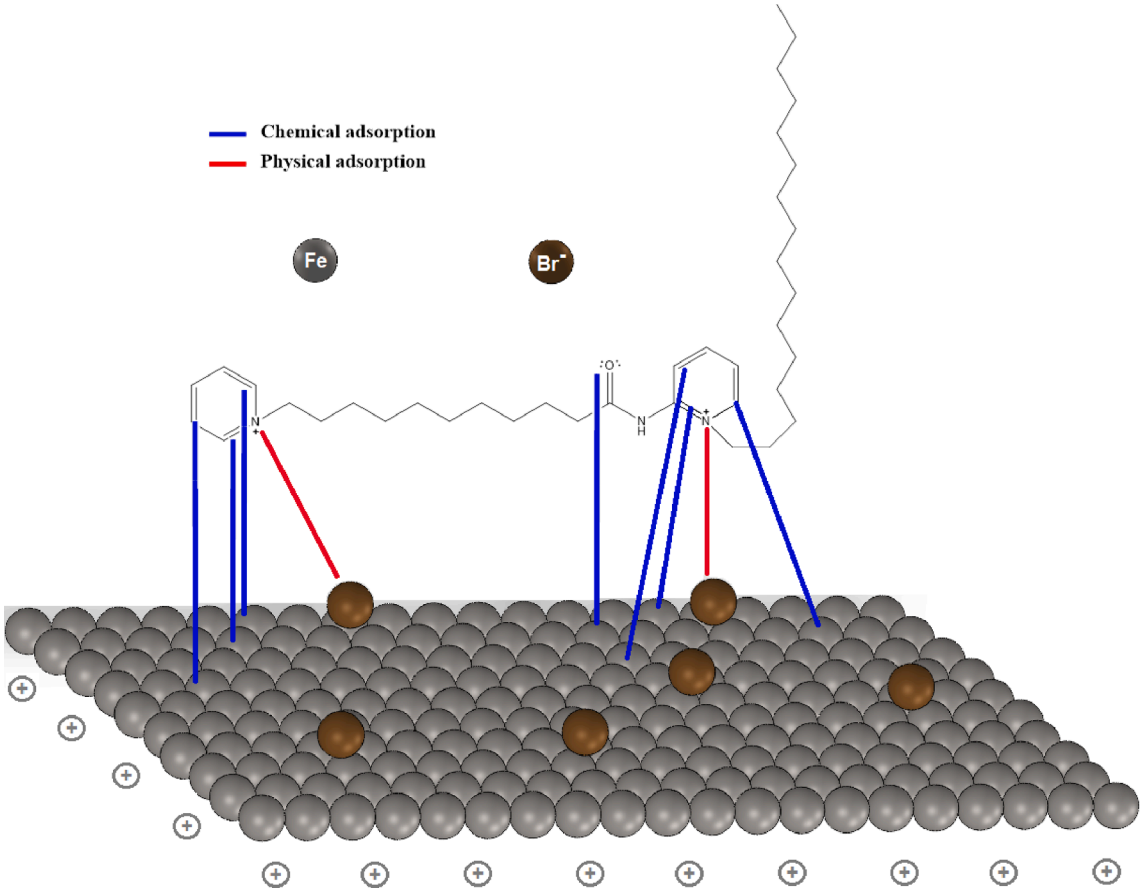

Fig. 8. Adsorption mechanism of HPUP on the metal surface.

show the plots of C_{inh} versus C_{inh} / θ. The K_{ads} values of cationic surfactant for different immersion times were calculated from the intersection of the linear graph in Fig. 7 and these value is given in Table 4. As seen in Table 4, K_{ads} values were determined as 36.32 x 10^5 M^{-1} for 6 h immersion time, 52.36 x 10^5 M^{-1} for 24 h immersion time, 259.01 x 10^5 M^{-1} for 48 h immersion time and 203.54 x 10^5 M^{-1} for 72 h immersion time. Except for 72 h of immersion time, we can generally say that K_{ads} values increased as the immersion time increased. That is, the ability of the surfactant to adsorb on the metal surface increased as the immersion time increased. From the K_{ads} values, it can be concluded that the strongest bond between the inhibitor molecule and the metal surface should be at 48 h immersion time [20]. To clarify this point, the Gibbs free energy values (ΔG^o_{ads}) of adsorption of cationic surfactant for different immersion times were calculated as shown in equation (14) below [41].

$$\Delta G^0_{ads} = -RTln(55.5xK_{ads}) \quad (14)$$

Where R is the universal gas constant, T is the absolute temperature and 55.5 is the molar concentration of water in solution. The ΔG^o_{ads} values for different imersion times are shown in Table 4. Negative Gibbs free energy values indicate that the adsorption of the surfactant to the metal surface occurs spontaneously at each immersion time. However, in a general approach, electrostatic interactions between charged molecules and the charged metal (physical adsorption) are effective at Gibbs free energy values up to –20 kJ mol^{-1}, while chemical adsorption involving electron sharing or transfer from inhibitor molecules to the metal surface is more effective at values more negative than –40 kJ mol^{-1} [42]. Looking at the ΔG^o_{ads} values calculated for 6, 24, 48, and 72 h immersion times in Table 4, it is possible to say that chemical adsorption is more effective in the adsorption of the inhibitor on the metal surface. In the adsorption mechanism shown in Fig. 8, it is shown how the di-cationic surfactant used as an inhibitor is attached to the metal surface by chemical and physical adsorption. When the structure of the synthesized di-cationic surfactant is examined, it is seen that there are two pyridinium rings as cationic groups. As seen in the adsorption mechanism given in Fig. 8, the metal surface, which was positively charged as a result of the oxidation of iron to the + 2 oxidation step in the anode reaction, turned negative by forming a dipole under the influence of chloride ions from the acid and bromide ions from the compound [27,43]. The negatively charged dipole and the positively charged nitrogen atoms of the inhibitors interact via electrostatic interaction (physical adsorption) and adsorb to the metal surface. In addition, the unpaired electron pairs in the oxygen atom and π electrons in the aromatic pyridinium ring in the structure of the compound interact with the empty d orbitals of the Fe element in the metal plates and attach to the

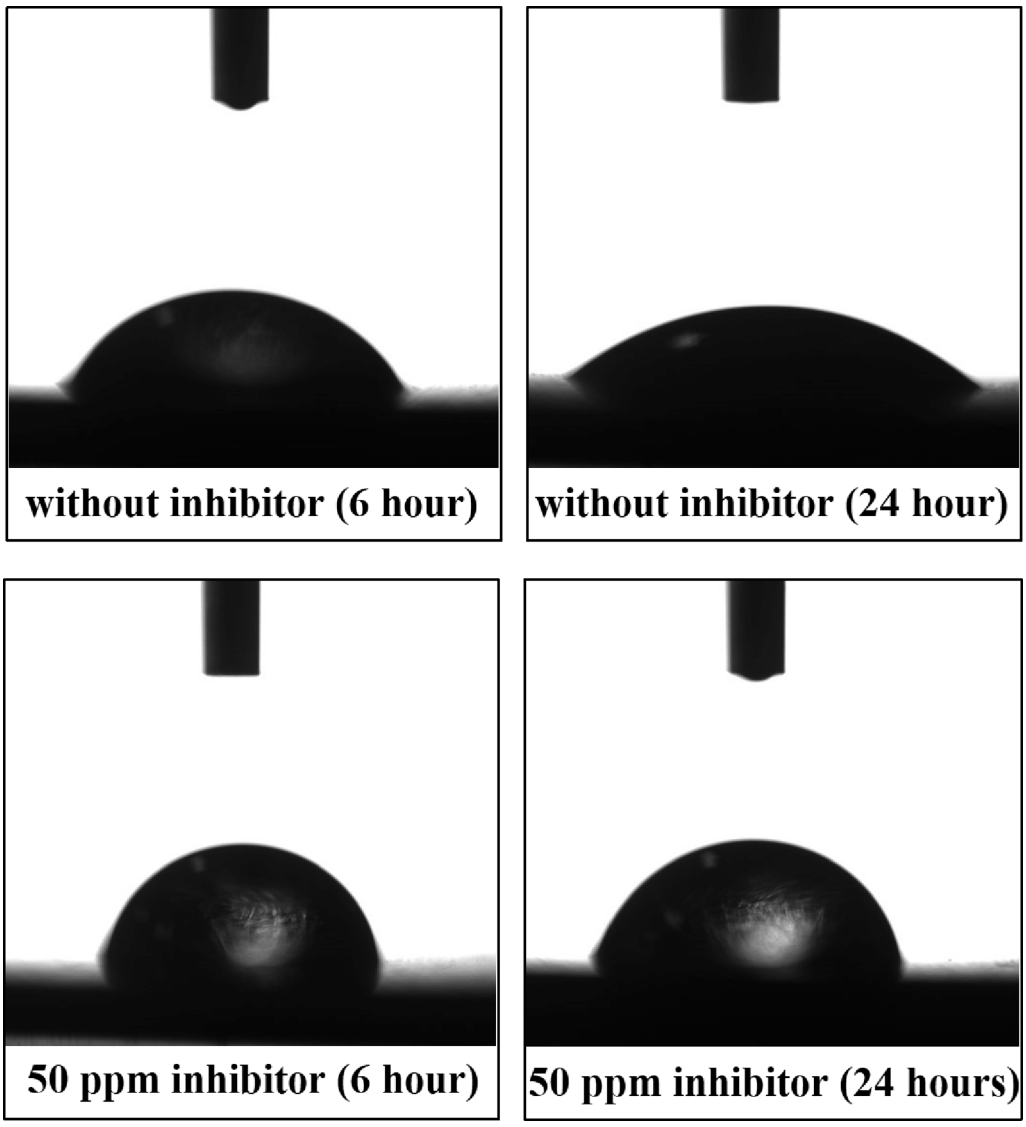

Fig. 9. Contact angle images determined on metal surfaces removed from 1.0 M HCl solution without inhibitor and containing 50 ppm di-cationic surfactants.

Table 5
Contact angle values determined for pure water dripped on the metal surface immersed in acid medium containing 50 ppm inhibitor and without inhibitor for 6 and 24 h at 25 °C.

Contact Angle Values			
Without inhibitor		50 ppm **HPUP**	
6 h	24 h	6 h	24 h
68.91° ± 0.31	40.35° ± 0.25	89.68° ± 0.66	81.27° ± 0.06

metal surface by chemical adsorption. As a result of both chemical and physical adsorption, the negative effect of acidic corrosive environment on the metal surface is prevented.

3.4. Contact angle measurement

The contact angle measurements determined by the pure water drop method dropped on the metal surface are visually shown in the Fig. 9. The contact angle values measured based on these images are given in the Table 5.

Thermodynamically, atoms tend to reduce their surface area. In this context, while the surface tensions of liquids are effective in wetting a surface, the first forces that come to mind are the cohesion forces between the molecules of the liquids and the adhesion forces between the liquids and the surface. As it is known, as the cohesion forces increase, liquids maintain their drop shape on the surface to which they are applied and their contact angles with the surface become large. However, if the adhesion forces of the liquid with the surface dominate the cohesion forces, the liquid spreads over the surface and the contact angle of the liquid with the surface becomes small. Looking at the contact angle values in Table 5, it was observed that the contact angle value of pure water dropped on the metal surface immersed in 1.0 M HCl solution with and without inhibitors for a longer time (24 h) decreased. This was an expected outcome. However, the contact angle on the metal surface removed from the acid containing inhibitor was larger because the di-cationic surfactant adsorbed on the metal surface over time made the metal surface hydrophobic. Since the metal surface removed from the corrosive medium without inhibitor is hydrophilic, a drop of water on this surface would spread more, and will reduce the contact angle with the surface. This situation is visually overwhelming in Fig. 9.

3.5. SEM and EDX analyses

The scanning electron microscopy (SEM) images in Fig. 10 show in detail how the metal surface changes before and after corrosion in 1.0 M

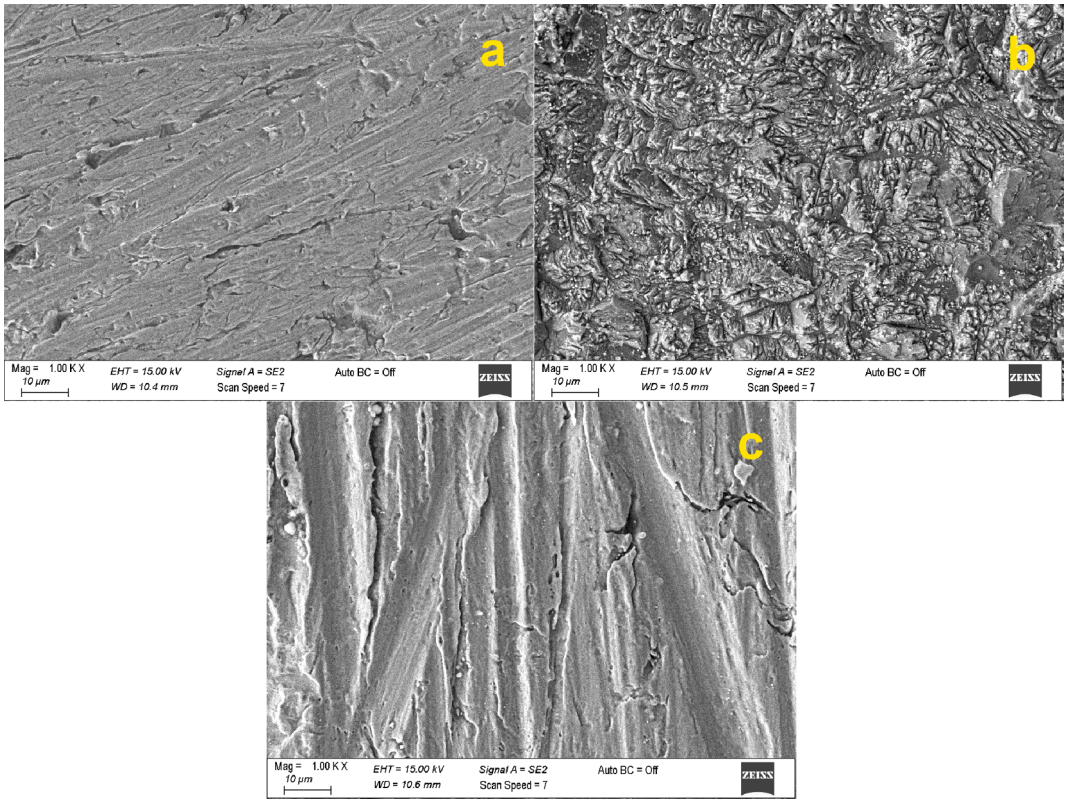

Fig. 10. Scanning electron microscopy (SEM) images of the metal surface **a)** before immersion in the corrosive 1.0 M HCl solution, **b)** after 24 h of immersion in 1.0 M HCl without inhibitor and **c)** after 24 h of immersion in 1.0 M HCl with 50 ppm inhibitor.

HCl solution, in the presence and absence of inhibitor. The images clearly show the differences in the morphology of the metal surface. This analysis allows us to visibly assess the effectiveness of inhibitors against corrosion.

The first SEM image (Fig. 10a) shows the metal surface before immersion in 1.0 M HCl solution. In the image, the metal surface appears to have a relatively smooth and linear structure. There are no obvious signs of deformation or corrosion on the surface except for small scratches and fine roughness. This indicates that the metal has a clean and smooth surface morphology. This state of the metal surface represents a pure state where corrosion has not started. At the micro scale, the deterioration of the metal surface is minimal and there are no obvious traces of

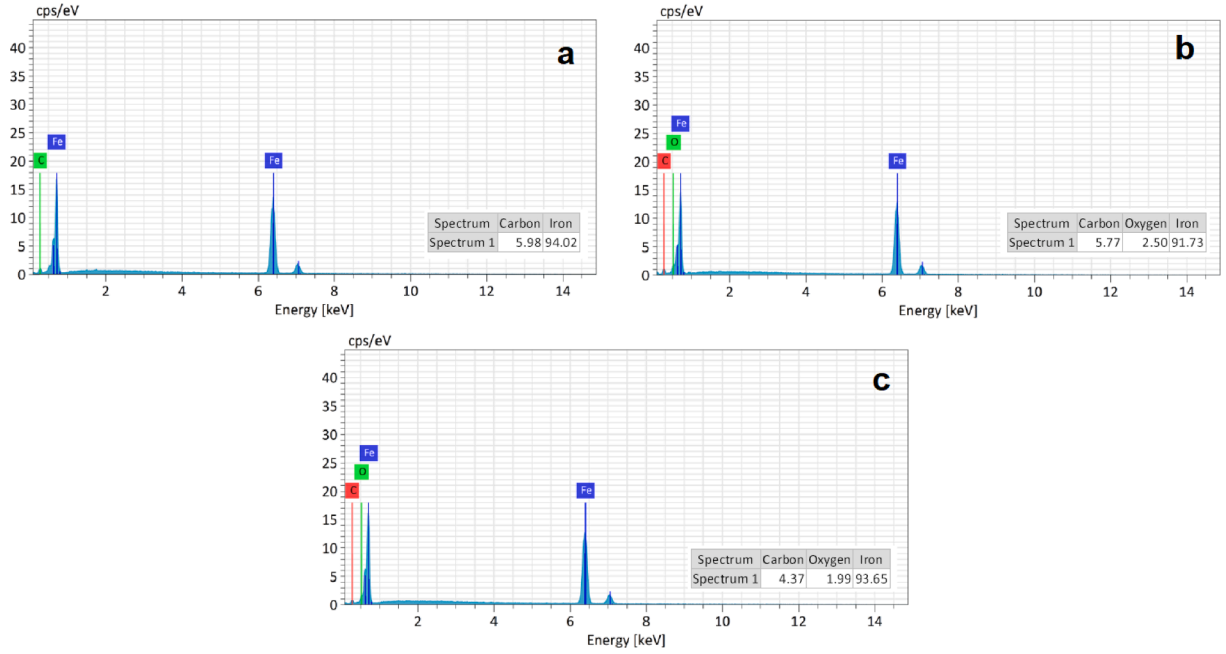

Fig. 11. Energy dispersive X-ray spectroscopy (EDX) spectra obtained for the metal surface **a)** before immersion in corrosive 1.0 M HCl solution **b)** after 24 h of immersion in 1.0 M HCl without inhibitor and **c)** after 24 h of immersion in 1.0 M HCl with 50 ppm inhibitor.

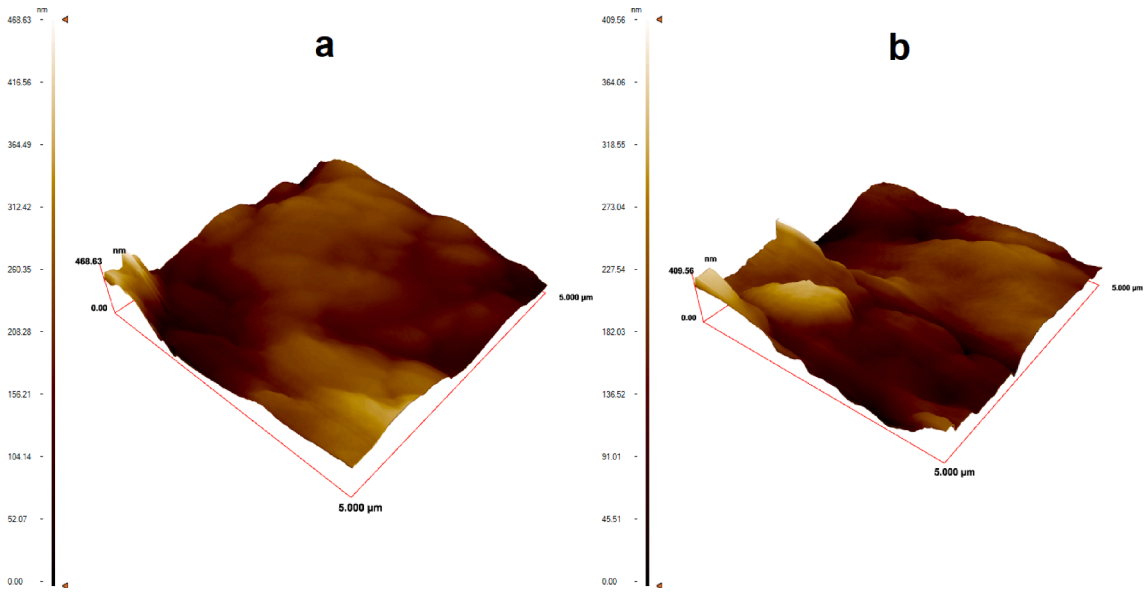

Fig. 12. AFM images for mild steel after exposure to 1.0 M HCl solution containing 50 ppm HPUP for (a) 24 h and (b) 72 h at 25 °C.

corrosion on the surface.

The second SEM image (Fig. 10b) shows the metal surface after 24 h of immersion in 1.0 M HCl solution without inhibitor. In the image, corrosion products are intensively observed on the metal surface. The surface is severely pitted and distorted. Corrosion has greatly affected the metal surface and made it highly irregular. The presence of roughnesses and corrosion products on the surface indicate that the metal was rapidly corroded in the HCl environment and the surface was substantially deformed. The surface of the metal was significantly damaged and had a non-homogeneous morphology. This image clearly shows that the metal corrodes very rapidly in the acidic environment in the absence of inhibitors and the surface is severely deformed.

The third SEM image (Fig. 10c) shows the state of the metal after immersion in 1.0 M HCl solution containing 50 ppm inhibitor for 24 h. It can be observed that the metal surface remains relatively smooth in the presence of the inhibitor and shows no obvious signs of corrosion. Although there are still some fine lines on the surface (due to sanding), it appears that the inhibitor has largely protected the metal surface. By forming a protective layer on the metal surface, the inhibitor significantly prevented surface degradation. The deformations on the surface are quite small compared to the severe corrosion symptoms observed in the case without inhibitor. This indicates that the inhibitor is effectively adsorbed on the metal surface and inhibits corrosion reactions. By preventing corrosion, the morphology of the metal surface was largely preserved and irregular deterioration was minimized. The inhibitor at 50 ppm concentration successfully protected the metal surface from the acidic environment and no serious deterioration of the surface occurred.

Energy Dispersive X-Ray Spectroscopy (EDX) analysis, shown in Fig. 11, examines the chemical composition of the elements on the metal surface. These analyses are used to understand the distribution of elements present on the surface and the effect of the presence of inhibitors on corrosion. EDX analyses show how the metal surface changes in the presence and absence of inhibitor in 1.0 M HCl solution in three different cases (before immersion, in the absence of inhibitor, in the presence of 50 ppm inhibitor).

In the EDX spectrum before immersion (Fig. 11a), iron (Fe) is predominant on the metal surface. Small amounts of carbon (C) are also observed as the metal used is low carbon steel. The high iron peak seen in the spectrum represents the main structure of the metal. This is the pure metal surface before a distinct protective layer forms on the surface [44].

In the second case (in the inhibitor-free environment) (Fig. 11b), the oxygen peak appeared prominently on the surface exposed to corrosion for 24 h in the inhibitor-free solution. This oxygen peak indicates that oxidation has started on the metal surface and corrosion is progressing. It is thought that Fe_2O_3 (iron II oxide) and other oxides (such as $Fe(OH)_3$) [45] are largely formed on the metal surface. The carbon and oxygen peaks represent the deterioration of the surface as corrosion progresses. The oxygen peak in particular indicates the oxidation of iron. The iron peak is still observed, but at a relatively low level due to the oxidation of iron on the surface. The progression of corrosion indicates that most of the iron on the surface has oxidized and destroyed the surface [20].

In the third case (with 50 ppm inhibitor) (Fig. 11c) the amounts of oxygen and carbon are lower than without inhibitor. This indicates that the inhibitor provides effective protection of the metal surface and prevents oxygen from electrochemically reacting with iron on the metal surface. For this reason, the iron peak increased again in the presence of 50 ppm inhibitor. This shows that the inhibitor protects the metal surface, preventing the iron from corroding, and that an inhibitor layer is formed on the surface instead of oxidation. The low levels of oxygen and other by-products (such as carbon) confirm that the inhibitor adsorbs to the surface and largely inhibits corrosion reactions. The inhibitor protected the surface by preventing the metal from corroding [44].

3.6. AFM

Atomic Force Microscopy (AFM) is an effective method for examining surface morphology at nano- to microscale levels. It has emerged as a valuable tool for studying the corrosion-inhibiting effects of inhibitors at the metal/solution interface. AFM provides crucial insights into surface properties, morphology, roughness, and elasticity [46]. The three dimensional AFM images of the steel surface exposed to 1.0 M HCl with 50 ppm of inhibitor solution for 24 h and 72 h are shown in Fig. 12a and Fig. 12b respectively. In Fig. 12, there is no AFM image on the metal surface removed from the inhibitor-free acid medium at the end of 24 and 72 h. This is because the metal surface removed from the inhibitor-free environment was so rough that the needle that scanned the surface while taking the AFM image was broken. Thus, unfortunately, no image could be taken for the inhibitor-free metal surface. As shown in Fig. 12, at the end of 24 (Fig. 12a) and 72 h (Fig. 12b), the average roughness on the metal surface removed from the acid medium containing inhibitor was determined as 49.37 and 52.77 nm, respectively. With the adsorption of inhibitor molecules on the metal surface, the surface treated with

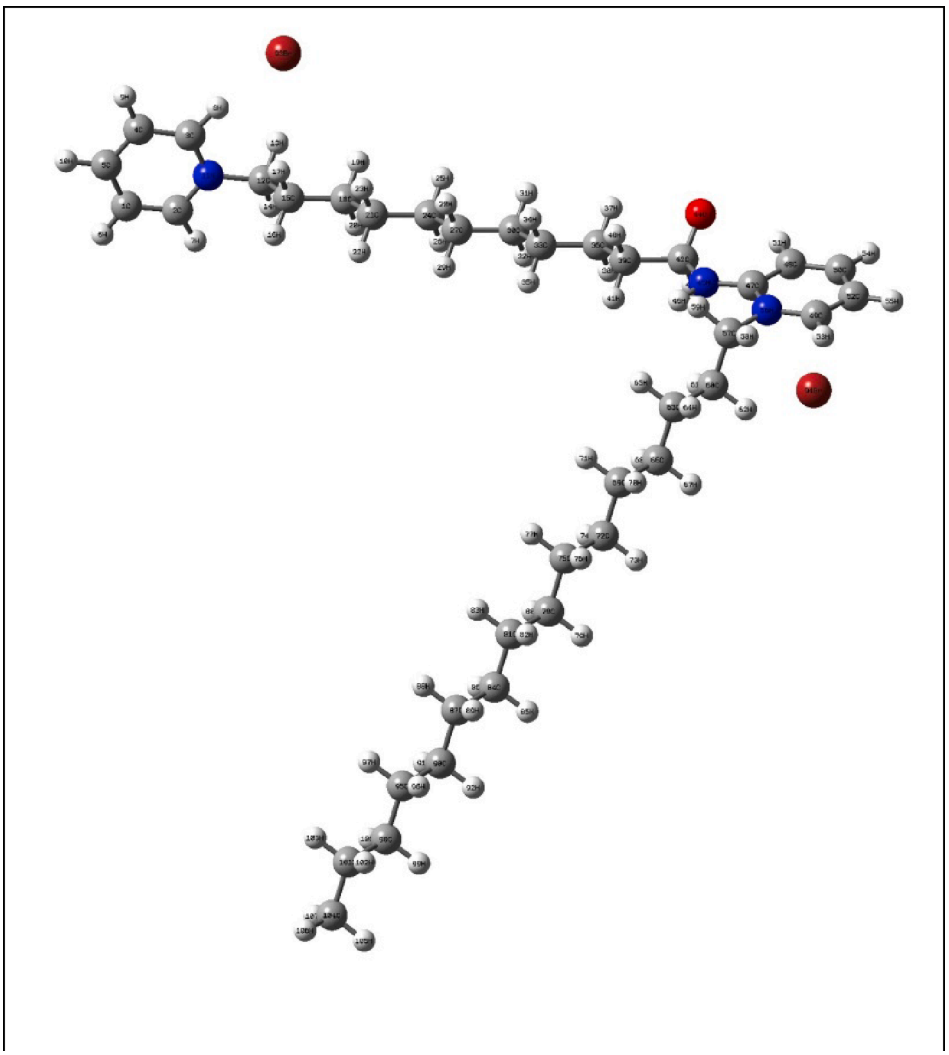

Fig. 13. Optimized structure of HPUP at the B3LYP/6–311++G(d,p) level.

inhibited 1.0 M HCl solution appears as a smoother and more uniform surface than the non-inhibited surface. In addition, the fact that the surface roughness averages are close to each other despite the increase in immersion time shows that the inhibitor is very firmly attached to the metal surface and is not easily desorbed.

3.7. Computer calculations

3.7.1. DFT

The optimized molecule of HPUP is shown in Fig. 13. In general, the prediction of the inhibition behavior of electronic systems rests upon the capability to assess an important property, namely the global reactivity. Chemical reactivity can be understood in terms of the HOMO and the LUMO. E_{HOMO} is often associated with the electron donating ability of a molecule, whereas E_{LUMO} indicates the ability of a molecule to accept electrons. Therefore, a high value of E_{HOMO} and a low value of E_{LUMO} could suggest efficient adsorption process. Thus, lower is the energy gap (ΔE); better is the electron transfer process. Graphical representations of the frontier molecular orbitals HOMO and LUMO are shown in Fig. 14. As is seen, the HOMO electron density of HPUP is concentrated on the carbon atoms neighbouring the pyridine ring together with the Br atom, whereas the LUMO receives a relatively smaller contribution from those carbon atoms, and delocalizes onto the C and N atoms of pyridine ring.

A molecule of high chemical hardness necessitates a significant energy input to undergo chemical alterations or interactions, attributed to a sizable energy barrier that hinders electron transfer. Conversely, a molecule denoted by substantial chemical softness, being the reciprocal of hardness, exhibits a marked propensity for electron transfer interactions. Switching to the assessment of nucleophilicity (ε) and electrophilicity (ω), which correspond to the capacity of an electron-rich molecule to donate electrons and an electron-deficient molecule to accept electrons, respectively. On the other hand, in the context of corrosion inhibition studies, the correlation between the fraction of electrons transferred (ΔN) and experimentally determined inhibition performance is of great importance. One has to keep in mind, however, that ΔN values are not an unequivocal expression of the number of electrons transferred between the donor and acceptor species. A positive value of ΔN (see. Table 6) indicates that the transfer of electrons can take place, while a negative value indicates that the opposite is true. Molecule exhibits a positive ΔN value, which implies a common propensity to facilitate electron transfer. The inhibitor does not exhibit a resistance to electron donation, suggesting that, in its interactions with other species, this compound is likely to participate in electron transfer reactions, which could influence its behavior in various chemical interactions.The electron-donating (ω^{+}) and electron-accepting (ω^{-}) power parameters for HPUP further substantiate the findings from the ΔN value, reinforcing the notion of the molecule's readiness to participate in electron transfer interactions.

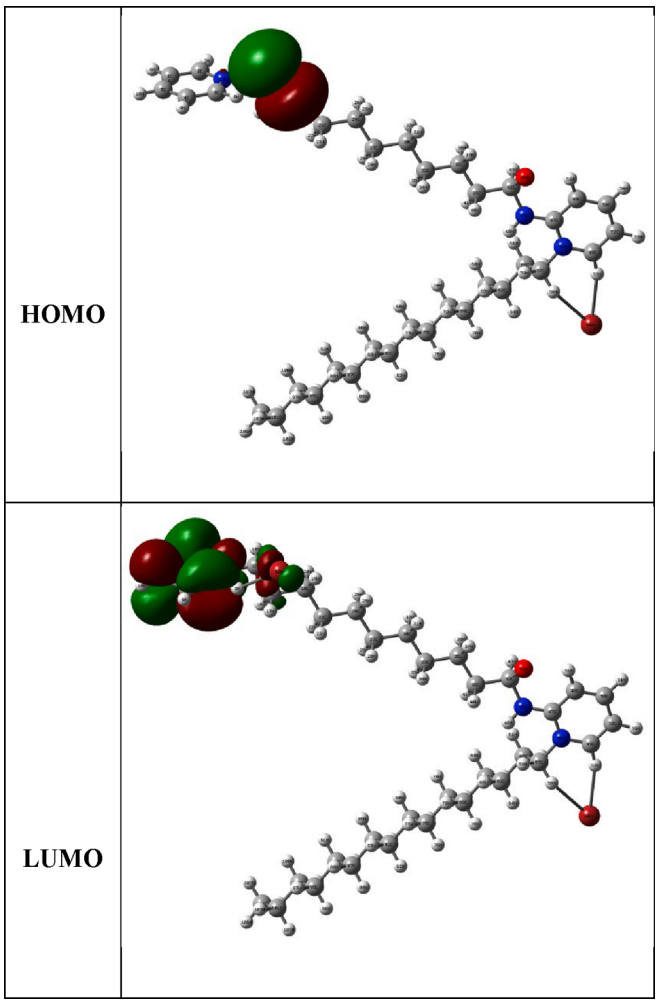

Fig. 14. Visualization of the HOMO and LUMO *iso*-surfaces as derived at the B3LYP/6–311++G(d,p) level.

Table 6
Molecular electronic parameters of HPUP.

Parameters	HPUP
E_{HOMO} (eV)	−5.157
E_{LUMO} (eV)	−3.217
ΔE (E_L-E_H) (eV)	1.940
ω	9.037
χ	4.187
η	0.970
σ	0.515
ε	0.111
ω^+	11.251
ω^-	7.064
ΔN	0.326

3.7.2. Monte Carlo simulation

Equilibrium configuration for the adsorption of 3b on Fe(110) are shown in Fig. 15. Fig. 15 shows the adsorption of **3** on Fe(110) without the competing corrosive electrolyte ions (Fig. 15a), and with corrosive electrolyte ions viewed from the side of the displaced ions (Fig. 15b) and viewed from the adjacent side (Fig. 15c). It could be observed that HPUP molecule adsorbed on Fe(110) using its heteroaromatic units and the adjoining aliphatic chain such that the terminal aliphatic chain could not be judged to have adsorbed directly on the substrate but might contribute electronically to the active units. The molecule of HPUP also displaced the corrosive electrolyte ions from its vicinity, suggesting that the adsorption of the inhibitor molecule on Fe(110) would block the corrosive ions from accessing the steel surface.

Adsorption energies were estimated, and the values are listed in Table 7. The results in Table 7 show that the adsorption of the inhibitor molecule on Fe(110) was accompanied by a substantial amount of adsorption energy (E_{ads}), which suggest that HPUP is an efficient inhibitor of acid corrosion of low carbon steel.

4. Conclusions

Di-cationic surfactant containing two cationic pyridinium rings was synthesized against general corrosion of mild steel surface in acidic medium (1.0 M HCl). Corrosion inhibition activities were investigated by electrochemical methods (OCP, Tafel extrapolarization and EIS). The inhibition efficiency results obtained by both potentiodynamic polarization method and electrochemical impedance spectroscopy method for the same concentrations of the inhibitor were found to be close and compatible with each other. With increasing inhibitor concentration, corrosion current densities (I_{corr}) decreased and corrosion resistance (R_{ct}) increased, resulting in a decrease in the corrosion rate on the metal surface and an increase in the corrosion inhibition efficiency of the di-cationic surfactant as the inhibitor concentration increased. As a result of contact angle measurements to prove that the synthesized di-cationic surfactant (HPUP) adsorbed on the metal surface, the contact angle values on the metal surface immersed in 1.0 M HCl solution containing 50 ppm inhibitor for 6 and 24 h were larger than those on the metal surface without inhibitor. This proved that HPUP adsorbed on the metal surface and made the metal surface hydrophobic. According to the K_{ads} and ΔG_{ads} values obtained from the Langmuir adsorption isotherm study of the inhibitor adsorbed on the metal surface, it was determined that the adsorption ability of the inhibitor was very high and it was mainly attached to the metal surface by chemical adsorption. Visual study of the adsorbed surfactant (HPUP) by scanning electron microscopy showed that corrosion products accumulated on the metal surface in the absence of inhibitor, while the metal surface was smoother in the inhibitor-containing environment, indicating that it was not affected by corrosion. This result was also supported by the change in the percentages of elements on the surface as a result of EDX analysis. Although the roughness ratio on the surface without inhibitor could not be determined at the end of 24 and 72 h by AFM analysis, it was observed that the roughness ratios on the metal surface containing inhibitor at the same immersion times were very close to each other. By examining the factors contributing to the understanding of corrosion inhibition by DFT analysis and explaining the effectiveness of the compound by the calculated descriptors, it can be suggested that the inhibitor is successful in protecting the metal surface against corrosion.

CRediT authorship contribution statement

Serkan Öztürk: Writing – review & editing, Writing – original draft, Visualization, Resources, Project administration, Methodology, Investigation, Formal analysis, Conceptualization. **Zafer Gültekin:** Writing – review & editing, Visualization, Software, Resources, Investigation, Formal analysis. **Gülşen Akgül:** Writing – review & editing, Resources, Investigation. **Gökhan Gece:** Writing – review & editing, Resources, Formal analysis. **Lukman O. Olasunkanmi:** Writing – review & editing, Resources, Formal analysis.

Declaration of competing interest

The authors declare that they have no known competing financial interests or personal relationships that could have appeared to influence the work reported in this paper.

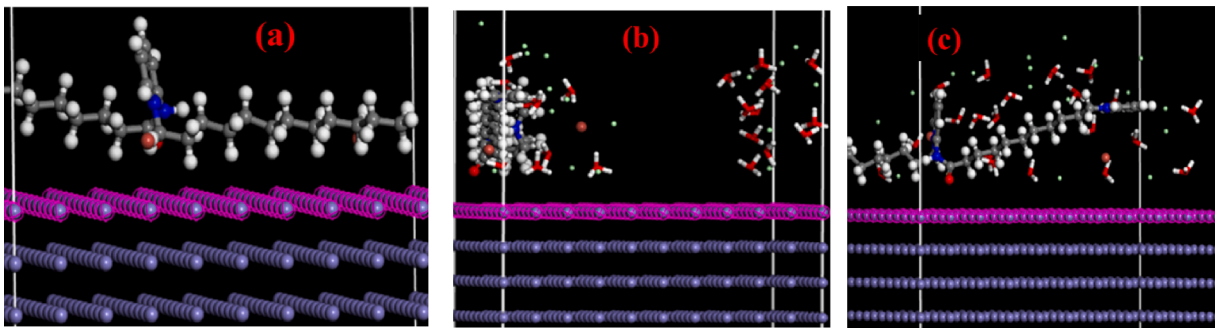

Fig. 15. Equilibrium configurations for the adsorption of HPUP on Fe(1 1 0) in the absence (a) and presence of 20 H_3O^+ and 20Cl^- ions, viewed from the side of displaced ions **(b)** and adjacent side **(c)**.

Table 7
Adsorption energies (E_{ads}) of HPUP on Fe(1 1 0) in the absence and presence of 20 H_3O^+ and 20Cl^-.

E_{ads} (kJ/mol)	Without Corrosive Ions	With Corrosive Ions (20 H_3O^+ and 20Cl^-)
$E_{(3/Fe(1\ 1\ 0))}$	−80.166	−231.794

Acknowledgements

This study was supported by Bursa Uludag University Scientific Research Projects Association under the project number FLO-2023-1452. We thank them for their support.

Appendix A. Supplementary data

Supplementary data to this article can be found online at https://doi.org/10.1016/j.apsusc.2025.162741.

Data availability

The authors do not have permission to share data.

References

[1] I.S. Pohrebova, T.M. Pylypenko, Inhibitors for acid corrosion of metals based on quaternary pyridinium salts containing carbonyl groups, Mater. Today Proc. 6 (2019) 192–201, https://doi.org/10.1016/j.matpr.2018.10.094.
[2] F. El-Hajjaji, R. Salim, M. Messali, et al., Insights of corrosion inhibitor based in pyridinium ionic liquids, Arab. J. Sci. Eng. 48 (2023) 7755–7770, https://doi.org/10.1007/s13369-022-07502-0.
[3] R. Salim, E.A. Abdelmalik, N. Benchat, et al., Corrosion behavior of a smart inhibitor in hydrochloric acid molar: Experimental and theoretical studies, Journal of Materials and Environmental Science 8 (2017) 3747–3758, https://www.jmaterenvironsci.com/Document/vol8/vol8_N10/394-JMES-2942-Salim.pdf.
[4] S. Tu, X. Jiang, L. Zhou, M. Duan, H. Wang, X. Jiang, Synthesis of N-alkyl-4-(4-hydroxybut-2-ynyl) pyridinium bromides and their corrosion inhibition activities on X70 steel in 5M HCl, Corros. Sci. 65 (2012) 13–25, https://doi.org/10.1016/j.corsci.2012.07.022.
[5] I. Öztürk, Corrosion protection of mild steel in cooling water systems with green polymeric inhibitors. (Doktora tezi, İstanbul Teknik Üniversitesi, Fen Bilimleri Enstitüsü, Polimer Bilim ve Teknolojisi Ana Bilim Dalı), İstanbul, Türkiye, 2020. https://polen.itu.edu.tr:8443/server/api/core/bitstreams/98751947-bf03-4830-8f3c-67544e69ce62/content.
[6] S. Sowmiah, J.M. Esperança, L.P. Rebelo, C.A. Afonso, Pyridinium salts: from synthesis to reactivity and applications, Org. Chem. Front. 5 (3) (2018) 453–493, https://doi.org/10.1039/C7QO00836H.
[7] L. Zhou, X. Jiang, Y. Li, Z. Chen, X. Hu, Synthesis and properties of a novel class of gemini pyridinium surfactants, Langmuir: the ACS J. Surfaces and Colloids 23 (2007) 11404–11408, https://doi.org/10.1021/la701154w.
[8] K. Shalabi, A.M. Helmy, A.H. El-Askalany, M.M. Shahba, New pyridinium bromide mono-cationic surfactant as corrosion inhibitor for carbon steel during chemical cleaning: Experimental and theoretical studies, J. Mol. Liq. 293 (2019) 111480, https://doi.org/10.1016/j.molliq.2019.111480.
[9] S. Öztürk, Z. Gültekin, N.A. Gültekin, G. Akgül, M. Alper, Synthesis of Di- and Tricationic Surfactants and Comparison of Their Activity on Oxidation of Metal in HCl Media, Prot. Met. Phys. Chem 59 (2023) 998–1009, https://doi.org/10.1134/S2070205123700958.
[10] G. Gece, The use of quantum chemical methods in corrosion inhibitor studies, Corros. Sci. 50 (2008) 2981–2992, https://doi.org/10.1016/j.corsci.2008.08.043.
[11] A. Kokalj, Molecular modeling of organic corrosion inhibitors: Calculations, pitfalls, and conceptualization of molecule - surface bonding, Corros. Sci. 193 (2021) 109650, https://doi.org/10.1016/j.corsci.2021.109650.
[12] M.M. Khalaf, A.H. Tantawy, K.A. Soliman, H.M. Abd El-Lateef, Cationic gemini-surfactants based on waste cooking oil as new 'green' inhibitors for N80-steel corrosion in sulphuric acid: A combined empirical and theoretical approaches, J. Mol. Struct. 1203 (2020) 127442, https://doi.org/10.1016/j.molstruc.2019.127442.
[13] A.H. Tantawy, K.A. Soliman, H.M. Abd El-Lateef, Experimental and computational approaches of sustainable quaternary bisammonium fluorosurfactants for corrosion inhibition as protective films at mild steel/H2SO4 interface, Colloids Surf A Physicochem Eng Asp 614 (2021) 126141, https://doi.org/10.1016/j.colsurfa.2021.126141.
[14] H.M. Abd El-Lateef, K. Shalabi, A.H. Tantawy, Corrosion inhibition of carbon steel in hydrochloric acid solution using newly synthesized urea-based cationic fluorosurfactants: experimental and computational investigations, New J. Chem. 41 (2020) 17791–17814, https://doi.org/10.1039/D0NJ04004E.
[15] A.H. Tantawy, K.A. Soliman, H.M. Abd El-Lateef, Novel synthesized cationic surfactants based on natural piper nigrum as sustainable-green inhibitors for steel pipeline corrosion in CO_2-3.5% NaCl: DFT, Monte Carlo simulations and experimental approaches, J. Cleaner Production 250 (2020) 119510, https://doi.org/10.1016/j.jclepro.2019.119510.
[16] Anonymous, Cold rolled low carbon steel flat products for cold forming—technical delivery conditions, German version EN 10130:2006, DIN (Deutsches Institut für Normung e.V.) Standard; 2007.
[17] S. Öztürk, Synthesis and corrosion inhibition behavior of novel amide-based quarternary di-cationic surfactants on carbon steel in HCl solutions, Prot. Met. Phys. Chem. 54 (2018) 953–962, https://doi.org/10.1134/S2070205118050167.
[18] Z. Gültekin, N.A. Gültekin, Recycling a Scrapped Magnetic Stirrer/Heater Using an Arduino Microcontroller, in: F. Özbaş Gerçeker, H. Akgül, H. Baba (Eds.), International Research in Science and Mathematics, Chapter 6, Serüven Publishing, İzmir, Turkey, 2022, p. 86. ISBN:978-625-6399-22-8.
[19] S. Öztürk, A. Yıldırım, M. Çetin, M. Tavaslı, Synthesis of quaternary, long-chain N-alkyl amides and their corrosion inhibition in acidic media, J. Surfactant Deterg. 17 (2014) 471–481, https://doi.org/10.1007/s11743-014-1566-5.
[20] H. Gerengi, M.M. Solomon, S. Öztürk, A. Yıldırım, G. Gece, E. Kaya, Evaluation of the corrosion inhibiting efficacy of a newly synthesized nitrone against St37 steel corrosion in acidic medium: experimental and theoretical approaches, Mater. Sci. Eng. C 93 (2018) 539–553, https://doi.org/10.1016/j.msec.2018.08.031.
[21] M. J. Frisch, G. W. Trucks, H. B. Schlegel, G. E. Scuseria, M. A. Robb, J. R. Cheeseman, G. Scalmani, V. Barone, B. Mennucci, G. A. Petersson, H. Nakatsuji, M. Caricato, X. Li, H. P. Hratchian, A. F. Izmaylov, J. Bloino, G. Zheng, J. L. Sonnenberg, M. Hada, M. Ehara, K. Toyota, R. Fukuda, J. Hasegawa, M. Ishida, T. Nakajima, Y. Honda, O. Kitao, H. Nakai, T. Vreven, J. A. Montgomery Jr., J. E. Peralta, F. Ogliaro, M. Bearpark, J. J. Heyd, E. Brothers, K. N. Kudin, V. N. Staroverov, R. Kobayashi, J. Normand, K. Raghavachari, A. Rendell, J. C. Burant, S. S. Iyengar, J. Tomasi, M. Cossi, N. Rega, J. M. Millam, M. Klene, J. E. Knox, J. B. Cross, V. Bakken, C. Adamo, J. Jaramillo, R. Gomperts, R. E. Stratmann, O. Yazyev, A. J. Austin, R. Cammi, C. Pomelli, J. W. Ochterski, R. L. Martin, K. Morokuma, V. G. Zakrzewski, G. A. Voth, P. Salvador, J. J. Dannenberg, S. Dapprich, A. D. Daniels, Ö. Farkas, J. B. Foresman, J. V. Ortiz, J. Cioslowski, D. J. Fox, Gaussian 09, Revision C.01,Gaussian, Inc., Wallingford CT, 2009.
[22] N. Wazzan, I.B. Obot, H. Lgaz, Z. Safi, O. Al-Qurashi, Multiscale computational modeling of phytochemicals for iron corrosion inhibition: Bridging DFT, SCC-DFTB, and molecular dynamics for eco-friendly solutions, J. Mol. Liq. 406 (2024) 125070, https://doi.org/10.1016/j.molliq.2024.125070.
[23] A.B. Anderson, S. Mehandru, Acetylene adsorption to Fe (100), (110), and (111) surfaces; structures and reactions, Surf. Sci. 136 (1984) 398–418, https://doi.org/10.1016/0039-6028(84)90620-4.
[24] A. Arya, E.A. Carter, Structure, bonding, and adhesion at the ZrC (1 0 0)/Fe (1 1 0) interface from first principles, Surf. Sci. 560 (1–3) (2004) 103–120, https://doi.org/10.1016/j.susc.2004.04.022.

[25] L.O. Olasunkanmi, E.E. Ebenso, Experimental and computational studies on propanone derivatives of quinoxalin-6-yl-4,5-dihydropyrazole as inhibitors of mild steel corrosion in hydrochloric acid, J. Colloid Interface Sci. 561 (2020) 104–116, https://doi.org/10.1016/j.jcis.2019.11.097.
[26] I.B. Onyeachu, I.B. Obot, A.A. Sorour, M.I. Abdul-Rashid, Green corrosion inhibitor for oilfield application I: Electrochemical assessment of 2-(2-pyridyl) benzimidazole for API X60 steel under sweet environment in NACE brine ID196, Corros. Sci. 150 (2019) 183–193, https://doi.org/10.1016/j.corsci.2019.02.010.
[27] S. Öztürk, Synthesis and corrosion inhibition effects of quinazolin-(3H)-4-one derivatives containing long-chain pyridinium salts on carbon steel in 1.5 M HCl, Prot. Met. Phys. Chem 53 (2017) 920–927, https://doi.org/10.1134/S2070205117050161.
[28] L.G. Qiu, A.J. Xie, Y.H. Shen, A novel triazole-based cationic gemini surfactant: synthesis and effect on corrosion inhibition of carbon steel in hydrochloric acid, Mater. Chem. Phys. 91 (2005) 269–273, https://doi.org/10.1016/j.matchemphys.2004.11.022.
[29] I. Aiad, M.A. Riya, S.M. Tawfik, M.A. Abousehly, Protection of carbon steel against corrosion in hydrochloric acid solution by some synthesized cationic surfactants, Prot. Met. Phys. Chem 52 (2016) 339–347, https://doi.org/10.1134/S2070205116020027.
[30] X. Yang, J. Wang, Z. Ren, W. Hu, Preparation and corrosion resistance of Ni-Fe layer double hydroxides superhydrophobic film on carbon steel, Colloids Surf A Physicochem. Eng. Asp 669 (2023) 131501, https://doi.org/10.1016/j.colsurfa.2023.131501.
[31] O. Mohamed, M. Hassan, M. Egilmez, W. Abuzaid, T. Ibrahim, M. Khamis, Corrosion behavior of CoCrNi/mild steel medium entropy alloy thin films, Mater. Today Commun. 30 (2022) 103015, https://doi.org/10.1016/j.mtcomm.2021.103015.
[32] M.A. Amin, M.A. Ahmed, H.A. Arida, F. Kandemirli, M. Saracoglu, T. Arslan, M. A. Basaran, Monitoring corrosion and corrosion control of iron in HCl by non-ionic surfactants of the TRITON-X series - part III, Immersion Time Effects and Theoretical Studies, Corrosion Science 53 (2011) 1895–1909, https://doi.org/10.1016/j. corsci.2011.02.007.
[33] S.A. Umoren, M.M. Solomon, Effect of halide ions on the corrosion inhibition efficiency of different organic species - a review, J. Ind. Eng. Chem. 21 (2015) 81–100, https://doi.org/10.1016/j.jiec.2014.09.033.
[34] E. Kamali Ardakani, E. Kowsari, A. Ehsani, Imidazolium-derived polymeric ionic liquid as a green inhibitor for corrosion inhibition of mild steel in 1.0 M HCl: experimental and computational study, Colloids and Surfaces A: Physicochem. Eng. Aspects 586 (2020) 124195, https://doi.org/10.1016/j.colsurfa.2019.124195.
[35] E. Ituen, O. Akaranta, A. James, Evaluation of performance of corrosion inhibitors using adsorption isotherm models: an overview, Chemical Science, Int. J. 18 (2017) 1–34, https://doi.org/10.9734/CSJI/2017/28976.
[36] C. Wang, C. Zou, Y. Cao, Electrochemical and isothermal adsorption studies on corrosion inhibition performance of β-cyclodextrin grafted polyacrylamide for X80 steel in oil and gas production, J. Mol. Struct. 1228 (2021) 129737, https://doi.org/10.1016/j.molstruc.2020.129737.
[37] S.S. Abd El Rehim, S.M. Sayyah, M.M. El-Deeb, S.M. Kamal, R.E. Azooz, Adsorption and corrosion inhibitive properties of P(2-aminobenzothiazole) on mild steel in hydrochloric acid media, Int. J. Indus. Chem. 7 (2016) 39–52, https://doi.org/10.1007/s40090-015-0065-5.
[38] Q. Zhang, Z. Gao, F. Xu, X. Zou, Adsorption and corrosion inhibitive properties of gemini surfactants in the series of hexanediyl-1,6-bis-(diethyl alkyl ammonium bromide) on aluminium in hydrochloric acid solution, Colloids Surf A Physicochem. Eng. Asp 380 (2011) 191–200, https://doi.org/10.1016/j.colsurfa.2011.02.035.
[39] H.M. Abd El-Lateef, A.M. Abu-Dief, L.H. Abdel-Rahman, E.C. Sañudo, N.N. Aliaga-Alcalde, Electrochemical and theoretical quantum approaches on the inhibition of C1018 carbon steel corrosion in acidic medium containing chloride using some newly synthesized phenolic Schiff bases compounds, J. Elec. Chem. 743 (2015) 120–133, https://doi.org/10.1016/j.jelechem.2015.02.023.
[40] A.S. El-Tabei, M.A. Hegazy, A.H. Bedair, N. El Basiony, M.A. Sadeq, Experimental and theoretical (DFT&MC) studies for newly synthesized cationic amphiphilic substance based on a naphthol moiety as corrosion inhibitor for carbon steel during the pickling process, J. Mol. Liq. 331 (2021) 115692, https://doi.org/10.1016/j.molliq.2021.115692.
[41] A. Liu, H. Tian, W. Li, W. Wang, X. Gao, P. Han, R. Ding, Delamination and selfassembly of layered double hydroxides for enhanced loading capacity and corrosion protection performance, Appl. Surf. Sci. 462 (2018) 175–186, https://doi.org/10.1016/j.apsusc.2018.08.109.
[42] A. Alizadeh, E. Khamehchi, A model for predicting size distribution and liquid drainage from micro-bubble surfactant multi-layer fluids using population balance, Colloid Polym. Sci. 293 (2015) 3419–3427, https://doi.org/10.1007/s00396-015-3678-5.
[43] A. Yıldırım, S. Öztürk, M. Çetin, Novel amide-based cationic surfactants as efficient corrosion inhibitors for carbon steel in HCl and H_2SO_4 media, J. Surfactant Deterg. 16 (2013) 13–23, https://doi.org/10.1007/s11743-012-1356-x.
[44] S. Öztürk, H. Gerengi, M.M. Solomon, G. Gece, A. Yıldırım, L.O. Olasunkanmi, Synthesis, characterization, and studies of the interfacial and anticorrosion properties of a ternary cationic ionic liquid on carbon steel in a molar concentration of hydrochloric acid: Experimental and computational insights, Colloids Surf A Physicochem. Eng. Asp 681 (2024) 132720, https://doi.org/10.1016/j.colsurfa.2023.132720.
[45] Y. Ji, B. Xu, W. Gong, Z. Zhang, Z. Jin, W. Ning, Y. Meng, W. Yang, Y. Chen, Corrosion inhibition of a new Schiff base derivative with two pyridine rings on Q235 mild steel in 1.0M HCl, J. Taiwan Inst. Chem. Eng. 66 (2016) 301–312, https://doi.org/10.1016/j.jtice.2016.07.007.
[46] N. Hilal, W.R. Bowen, L. Alkhatib, O.A. Ogunbiyi, Review of atomic force microscopy applied to cell interactions with membranes, Chem. Eng. Res. Des. 84 (2006) 282–292, https://doi.org/10.1205/cherd05053.